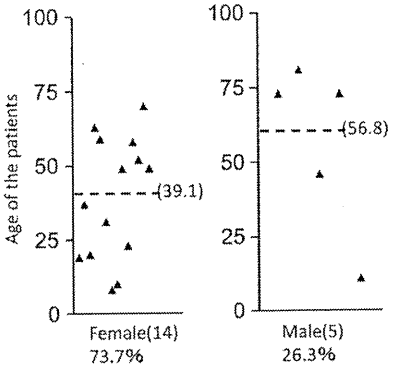

FIG. 2. Ages and genders of BU patients in Japan.

401-bp (*hsp65*) fragments. Ten clinical isolates were compared to six reference strains: *M. ulcerans* ITM 98-912, *M. ulcerans* ATCC 19423^T, *M. ulcerans* Agy99 (25), *Mycobacterium marinum* ATCC 927^T, *M. marinum* clinical isolate LRC 112509, and *Mycobacterium pseudoshottsii* JCM 15466^T. A similarity search was also performed with other mycobacterial reference strains and the 10 clinical strains using the DNA Data Bank of Japan (DDBJ) (8). Phylogenetic analyses were performed using the MEGA software package, version 4.0.2 (build 4028) (29). A tree was constructed using the neighbor-joining method with Kimura's two-parameter distance correction model with 1,000 bootstrap replications.

Finally, primers for eight pMUM001 sequences that encode toxic lipid mycolactone-producing enzymes (26) were used to compare the PCR products of the 10 clinical isolates, *M. ulcerans* ITM 98-912, *M. ulcerans* ATCC 19423^T, *M. ulcerans* Agy99, and *M. pseudoshottsii* JCM 15466^T.

DNA-DNA hybridization assay. A commercially available DNA-DNA hybridization method (DDH Mycobacteria kit; Kyokuto Pharmaceutical Industrial, Tokyo, Japan) was used to identify mycobacterial species isolated from patients (13). The 18 strains in the *Mycobacterium* reference panel included *M. marinum* but not *M. ulcerans*, *M. ulcerans* subsp. *shinshuense*, or *M. pseudoshottsii*.

Growth characteristics and biochemical assay. Culture growth characteristics were determined, and identification was performed, as described previously (16) for 10 of the 11 mycobacterial isolates recovered from patients.

Assay for susceptibility to antimycobacterial drugs. The susceptibilities of the clinical isolates to antibiotics *in vitro* were determined by microdilution (33) using the BrothMIC NTM kit (Kyokuto Pharmaceutical Industrial Co. Ltd., Tokyo, Japan), with modification of the incubation temperature (32°C) and period (2 to 3 weeks). MIC testing was performed in triplicate on different days, with two of three matching MICs used as the criterion for MIC determination.

Nucleotide sequence accession numbers. The DNA sequences of the 16S rRNA (1,475-bp), *hsp65* (401-bp), *rpoB* (315-bp), and ITS (272-bp) fragments from the reference strains (*M. ulcerans* ITM 98-912, *M. ulcerans* ATCC 19423^T, *M. ulcerans* Agy99, *M. marinum* ATCC 927^T, *M. marinum* clinical isolate LRC 112509, and *M. pseudoshottsii* JCM 15466^T) and 10 clinical isolates have been deposited in the International Nucleotide Sequence Database (INSD) through the DDBJ under accession numbers AB548711 to AB548734 and AB624260 to AB624295.

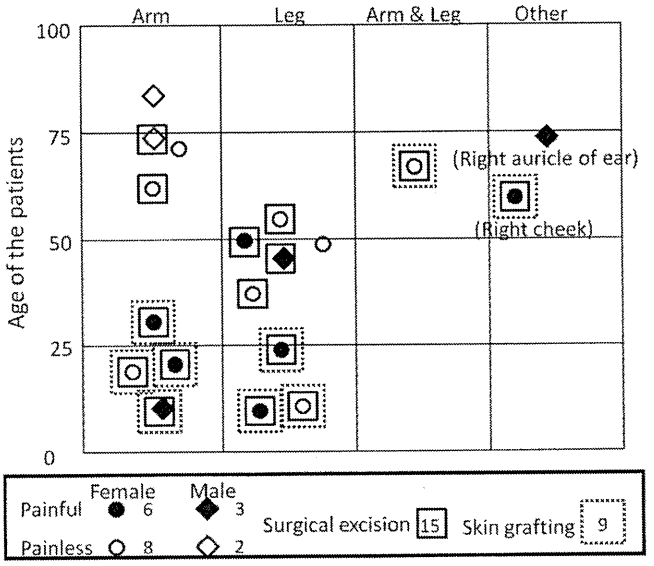

FIG. 4. Localization, pain, and surgical treatment of ulcer lesions by age and gender.

RESULTS

Epidemiology. Nineteen BU cases from Japan have been reported to the WHO BU committee as of December 2010. Many of the *M. ulcerans*-related reports of BU have originated in tropical wetlands. However, Japan is located in eastern Asia, and the majority of the country is covered by mountainous terrain. The 19 cases were distributed between latitudes 34°N and 38°N, in a typical temperate region of Japan.

There was no geographic focal point in the distribution of the BU cases. However, all of the patients lived on Honshu, the largest island of Japan. Seven cases were found in the Chugoku region (western Honshu), 6 in the Chubu region (central Honshu), 4 in the Kinki region (between Chugoku and Chubu), 1 in the Tohoku region (northern Honshu), and 1 in the Kanto region (eastern Honshu) (Fig. 1).

Fourteen (73.7%) subjects were female, and 5 (26.3%) were male. The average age was 39.1 years (range, 8 to 70 years) for the females and 56.8 years (range, 11 to 81 years) for the males (Fig. 2). Despite careful and precise patient interviews, none of the cases could be linked to an aquatic environment.

The affected areas were on exposed sites, such as arms (8

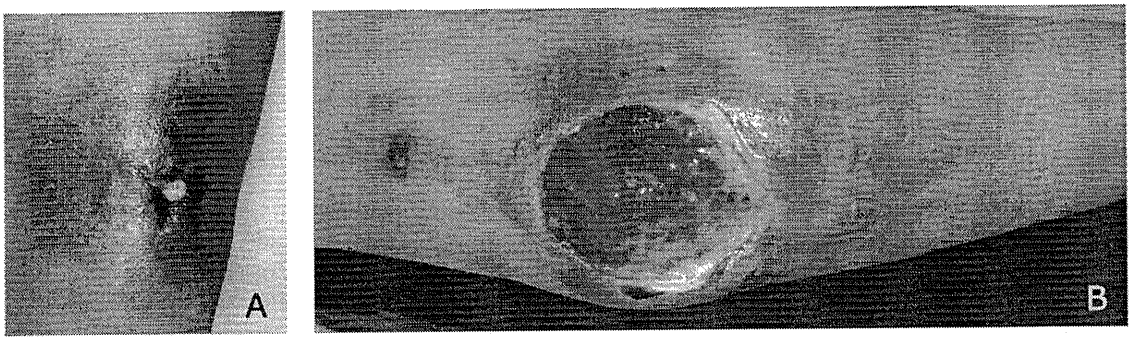

FIG. 3. (A) Buruli ulcer case 8: a category I ulcer on the right forearm. (B) Buruli ulcer case 3: a category II ulcer on the right elbow extensor surface.

TABLE 2. IS*2404* detection in 19 cases of BU in Japan

Case no.	Yr of diagnosis	Origin (region)	Sample type			Isolation period[c]
			Tissue sample[a]	Paraffin section[b]	Isolate	
1	1980	Chubu	NT	NT	P	4 wk
2	2004	Chubu	NT	NT	P	S
3	2006	Chugoku	P	P	P	11 wk
4	2005	Kinki	NT	NT	P	6 wk
5	2007	Chubu	P	P	P	8 wk
6	2007	Chubu	NT	NT	P	S
7	2007	Kinki	NT	NT	P	S
8	2008	Chubu	P	NT	P	11 mo
9	2008	Chugoku	P	NT	NT	NT
10	2009	Chugoku	P	NT	NT	NT
11	2009	Chugoku	P	P	NT	NT
12	2009	Chugoku	P	P	NT	NT
13	2009	Chugoku	NT	P	P	12 wk
14	2009	Tohoku	P	NT	NT	NT
15	2010	Kinki	P	NT	NT	6 wk
16	2010	Kanto	P	P	NT	NT
17	2010	Chubu	P	P	P	5 wk
18	2010	Kinki	P	P	NT	NT
19	2010	Chugoku	P	P	NT	NT

[a] Frozen or fresh skin biopsy sample. NT, not tested; P, positive.
[b] Sliced from a formalin-fixed, paraffin-embedded skin biopsy sample.
[c] S, isolation was successful, but the incubation period was uncertain.

cases), legs (8 cases), the right auricle of the ear (1 case), the right cheek (1 case), and both arms and legs (1 case). While skin ulcer lesions were present in all cases, most were smaller than 5 cm in diameter and were classified as category I (Fig. 3A) (36). In one severe case, the patient presented with a progressive ulcer larger than 10 cm in diameter on the extensor surface of the right elbow, which fell into category II (Fig. 3B). Nine patients (47%) experienced pain, although in many reported cases, BU is painless or only slightly painful (Fig. 4).

Genotypic analysis. PCR screening to detect IS*2404* gave a positive result for at least one of three sample types in all 19 cases. We should note that fresh tissue samples were the source of the template for 13 cases, while formalin-fixed, paraffin-embedded specimens were also used for 9 cases, and all were positive (Table 2). Mycobacteria were successfully isolated in 11 of the 19 cases; however, further bacteriological tests, including genotypic analysis, were performed on 10 available isolates.

The 16S rRNA gene sequences (1,475 bp) of these isolates were identical to each other but partially different from those of *M. ulcerans*, *M. marinum*, and *M. pseudoshottsii* (Table 3). The *hsp65* (401-bp), *rpoB* (315-bp), and internal transcribed spacer (ITS) (272-bp) sequences were also identical among isolates. Sequence analysis identified *M. ulcerans* subsp. *shinshuense* as the bacterium in the clinical samples. Phylogenetic trees based on 16S rRNA and *hsp65* gene sequences showed a close relationship between *M. ulcerans* subsp. *shinshuense* and *M. ulcerans* (Fig. 5A and B). A phylogenetic analysis of the 16S–23S intergenic spacer region showed no differences between *M. ulcerans* subsp. *shinshuense*, *M. marinum*, and *M. ulcerans* and found that *M. pseudoshottsii* is a close relative (Fig. 5C). In contrast, the tree based on the *rpoB* gene showed a closer relationship of *M. ulcerans* subsp. *shinshuense* to *M. marinum* and *M. pseudoshottsii* than to *M. ulcerans*, supporting the premise that *M. ulcerans* subsp. *shinshuense* is distinct from *M. ulcerans* (Fig. 5D).

Next, amplification of eight pMUM001-associated genes was used to determine whether these isolates had genes that encode toxic lipid mycolactone-producing enzymes. All isolates

TABLE 3. Comparison of 16S rRNA gene sequences of 10 *M. ulcerans* subsp. *shinshuense* isolates and related mycobacterial strains

Strain	Country	Nucleotide(s) at the following *Escherichia coli* 16S rRNA gene sequence position(s):								
		95	487–488	492	969	1007	1215	1247	1288	1449–1451[a]
M. ulcerans subsp. *shinshuense*										
ATCC 33728	Japan	T	GG	G	A	G	T	G	G	ACCC---TTTG
JATA753	Japan	T	GG	G	A	G	T	G	G	ACCC---TTTG
0401	Japan	T	GG	G	A	G	T	G	G	ACCC---TTTG
0501	Japan	T	GG	G	A	G	T	G	G	ACCC---TTTG
0701	Japan	T	GG	G	A	G	T	G	G	ACCC---TTTG
0702	Japan	T	GG	G	A	G	T	G	G	ACCC---TTTG
0703	Japan	T	GG	G	A	G	T	G	G	ACCC---TTTG
0801	Japan	T	GG	G	A	G	T	G	G	ACCC---TTTG
0901	Japan	T	GG	G	A	G	T	G	G	ACCC---TTTG
1001	Japan	T	GG	G	A	G	T	G	G	ACCC---TTTG
M. ulcerans										
ITM 98-912	China	T	GG	G	A	G	T	G	G	ACCC---TTTG
ATCC 19423^T	Australia	T	GG	A	A	G	T	G	C	ACCC---TTTG
Agy99	Ghana	T	GG	A	A	G	T	G	C	ACCCTTTTTTG
M. marinum										
ATCC 927^T	United States	T	GG	A	A	G	T	A	A	ACCC---TTTG
112509	Japan	T	GG	A	A	G	T	A	A	ACCC---TTTG
M. pseudoshottsii JCM 15466^T	United States	C	GA	A	G	T	C	A	A	ACCC---TTTG

[a] Hyphens indicate gaps.

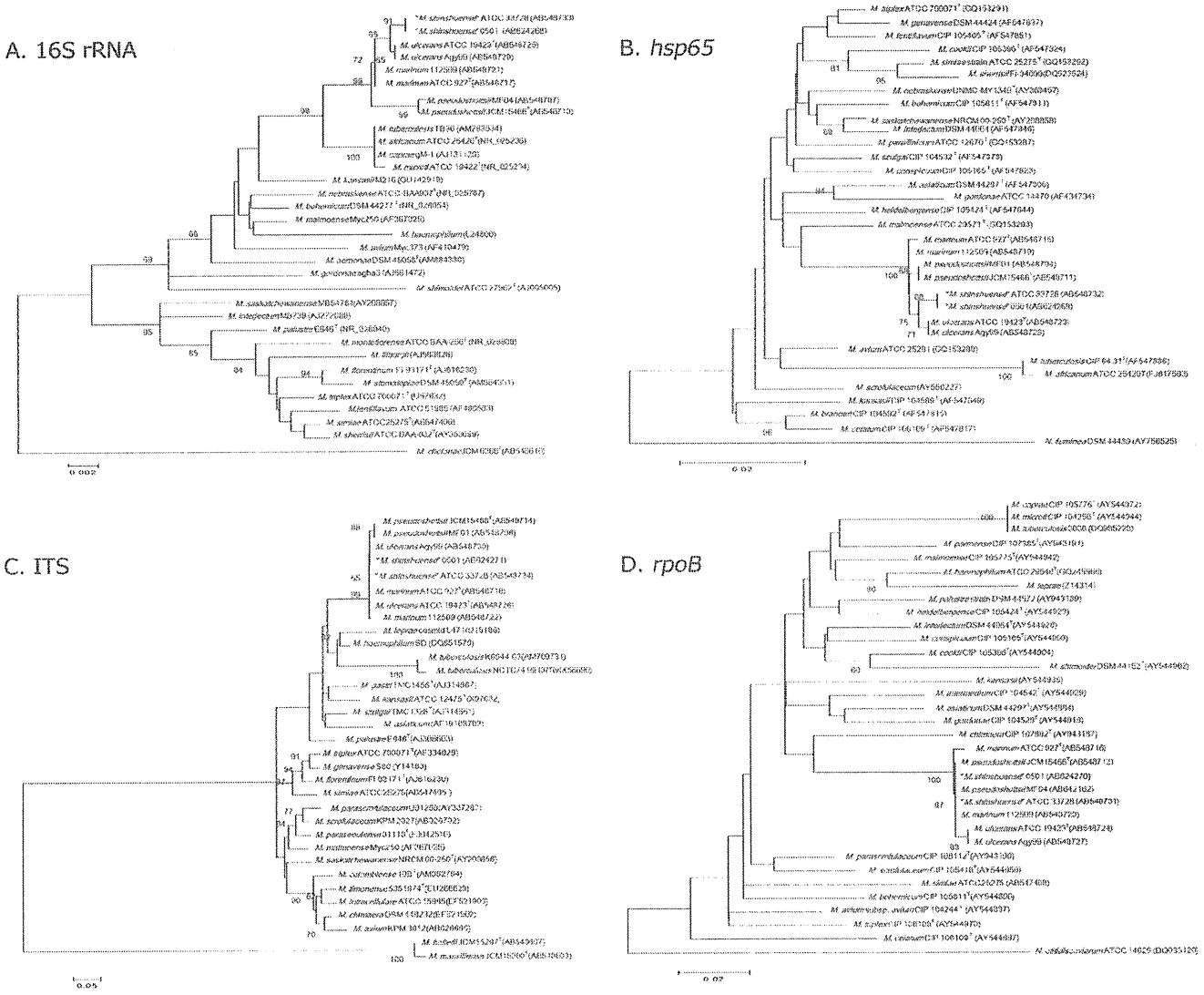

FIG. 5. Phylogenetic analyses of *M. ulcerans* subsp. *shinshuense* based on the 16S rRNA gene (A), the *hsp65* gene (B), the 16S–23S intergenic spacer region (C), and the *rpoB* gene (D).

showed positive results, but as previously reported, the band representing the serine/threonine protein kinase (STPK) gene was absent in *M. ulcerans* subsp. *shinshuense* strains (16). However, this phenomenon was also observed with one strain of *M. ulcerans*, ITM 98-912, that was isolated in China (4). All eight bands were detected in the *M. ulcerans* strains isolated from Australia and Ghana. *M. pseudoshottsii* lacked the band representing P450, but the other seven bands were successfully amplified (Table 4).

A commercially available DNA-DNA hybridization assay was used to verify species identity. The kit contained a reference panel of 18 mycobacterial strains that included *M. marinum* but not *M. ulcerans*, *M. ulcerans* subsp. *shinshuense*, or *M. pseudoshottsii*. All 10 isolates showed clear positive signals for *M. marinum* (Table 5, rightmost column).

Biochemical characteristics. The 10 isolates exhibited the same characteristics: rough colonies and yellow pigmentation, even when grown in the dark. The slowly growing mycobacterium formed visible colonies at 25°C and 32°C on a 2% Ogawa egg slant, but not at 37°C or 42°C. No growth was seen on a medium supplemented with 500 μg/ml *p*-nitrobenzoic acid or 5% NaCl. The isolates were negative for niacin, nitrate reduction, arylsulfatase (3 days), Tween 80 hydrolysis, pyrazinamidase, and iron uptake but were positive for semiquantitative catalase and 68°C catalase and urease. Comparisons between *M. ulcerans* subsp. *shinshuense*, *M. ulcerans*, and *M. marinum* are summarized in Table 5. These results were in accordance with those of a previous report (22) except for the positive result of *M. ulcerans* subsp. *shinshuense* on the urease test.

Drug susceptibility assays. Table 6 shows the results of testing of the susceptibilities of *M. ulcerans* subsp. *shinshuense* ATCC 33728 and *M. ulcerans* subsp. *shinshuense* clinical isolate 0501 to antimicrobial agents. These isolates exhibited high susceptibilities to streptomycin, kanamycin, levofloxacin, and clarithromycin. Notably, *M. ulcerans* subsp. *shinshuense* was more susceptible to streptomycin, kanamycin, and clarithromy-

TABLE 4. PCR detection of eight pMUM001-associated genes in 10 *M. ulcerans* subsp. *shinshuense* isolates and related mycobacterial strains

Strain	Country	Presence or absence of the following pMUM001 marker gene[a]:							
		repA	*parA*	STPK	*mls* (load)	*mlsAT(II)*	TEII	KSIII	P450
M. ulcerans subsp. *shinshuense*									
ATCC 33728	Japan	+	+	−	+	+	+	+	+
JATA753	Japan	+	+	−	+	+	+	+	+
0401	Japan	+	+	−	+	+	+	+	+
0501	Japan	+	+	−	+	+	+	+	+
0701	Japan	+	+	−	+	+	+	+	+
0702	Japan	+	+	−	+	+	+	+	+
0703	Japan	+	+	−	+	+	+	+	+
0801	Japan	+	+	−	+	+	+	+	+
0901	Japan	+	+	−	+	+	+	+	+
1001	Japan	+	+	−	+	+	+	+	+
M. ulcerans									
ITM 98-912	China	+	+	−	+	+	+	+	+
ATCC 19423^T	Australia	+	+	+	+	+	+	+	+
Agy99	Ghana	+	+	+	+	+	+	+	+
M. pseudoshottsii JCM 15466^T	United States	+	+	+	+	+	+	+	−

[a] +, present; −, absent. STPK, serine/threonine protein kinase; TEII, type II thioesterase; KSIII, type III ketosynthase.

cin than the *M. ulcerans* reference strains. Like the *M. ulcerans* reference strains, *M. ulcerans* subsp. *shinshuense* was susceptible to amikacin but resistant to ethambutol, isoniazid, and ethionamide.

Treatment. The 19 patients were treated with various antibiotic regimens. Clarithromycin was effective for many of the Japanese patients (12 cases). Rifampin was successful in the first case and was used thereafter in 9 cases. Attempts at treatment with other medications, alone and in combinations, were also made (Table 7). In 2 cases, the initial choice of antibiotics was ineffective, and they were changed. In 2 other cases, the antibiotic treatment was discontinued due to adverse effects. In addition to antibiotic treatment, 13 patients underwent surgical excision, and 9 needed skin grafting (Fig. 4). No relapses had been reported as of March 2011.

DISCUSSION

This is the first report that comprehensively analyzes both the genotypic and the biochemical profiles of a causative agent of Buruli ulcer in Japan. It is noteworthy that BU in Japan was induced by *Mycobacterium ulcerans* subsp. *shinshuense*, not by *M. ulcerans*. We compared certain characteristics of *M. ulcerans* and *M. ulcerans* subsp. *shinshuense* by several analyses. They are relatively similar; detection of IS*2404* by PCR was the most important test for early diagnosis and differential diag-

TABLE 5. Bacteriological characteristics of 10 *M. ulcerans* subsp. *shinshuense* isolates and closely related mycobacterial strains

Strain	Country	Biochemical characteristic							Identification of *M. marinum*[b]
		Growth rate	Colony morphology	Pigment in dark	Urease activity	Tween 80 hydrolysis	PZase[a] activity	MPB64 production	
M. ulcerans subsp. *shinshuense*									
ATCC 33728	Japan	Low	Rough	Yellow	+	−	−	−	+
JATA753	Japan	Low	Rough	Yellow	+	−	−	−	+
0401	Japan	Low	Rough	Yellow	+	−	−	−	+
0501	Japan	Low	Rough	Yellow	+	−	−	−	+
0701	Japan	Low	Rough	Yellow	+	−	−	−	+
0702	Japan	Low	Rough	Yellow	+	−	−	−	+
0703	Japan	Low	Rough	Yellow	+	−	−	−	+
0801	Japan	Low	Rough	Yellow	+	−	−	−	+
0901	Japan	Low	Rough	Yellow	+	−	−	−	+
1001	Japan	Low	Rough	Yellow	+	−	−	−	+
M. ulcerans									
ITM 98-912	China	Low	Rough	Yellow	+	−	−	−	+
ATCC 19423^T	Australia	Low	Rough	None	−	−	−	−	+
Agy99	Ghana	Low	Rough	Yellow	−	−	−	−	+
M. marinum ATCC 927^T	United States	Medium	Smooth	None	+	+	+	−	+

[a] PZase, pyrazinamidase.
[b] By use of the DDH Mycobacteria kit (Kyokuto Pharmaceutical Industrial, Tokyo, Japan).

TABLE 6. Drug susceptibility test results

Antimycobacterial drug[a]	MIC (μg/ml) for:			
	M. ulcerans subsp. *shinshuense*		*M. ulcerans*	
	ATCC 33728	0501	ATCC 19423^T	Agy99
SM	0.125	0.25	1	4
EB	16	8	16	128
KM	0.25	0.25	1	1
INH	8	8	>32	>32
RFP	0.06	0.06	0.06	0.06
LVFX	0.25	0.5	0.5	8
CAM	0.03	0.06	0.25	0.125
TH	16	8	16	16
AMK	0.5	0.5	0.5	0.5

[a] SM, streptomycin; EB, ethambutol; KM, kanamycin; INH, isoniazid; RFP, rifampin; LVFX, levofloxacin; CAM, clarithromycin; TH, ethionamide; AMK, amikacin.

TABLE 7. Antibiotic treatment regimens for BU cases

Regimen[a]	No. of cases
Single drug	
CAM	2
MINO	1
RFP	1
Two drugs	
CAM, RFP	2
ITZ, MINO	1
LVFX, MINO	1
Three drugs	
CAM, LVFX, RFP	3
CAM, CFPN-PI, NFLX	1
CFPN-PI, LVFX, MINO	1
CAM, MINO, NFLX	1
GRNX, LVFX, MINO	1
Four drugs (EB, LVFX, RFP, SM)	1
Six drugs	
AZM, CAM, CPFX, LVFX, MINO, RFP	1
CAM, EB, GFLX, INH, RFP, SM	1
CAM, CPFX, LVFX, MINO, PZFX, RFP	1

[a] AZM, azithromycin; CAM, clarithromycin; CFPN-PI, cefcapene-pivoxil; CPFX, ciprofloxacin; EB, ethambutol; GFLX, gatifloxacin; GRNX, garenoxacin; INH, isoniazid; ITZ, itraconazole; LVFX, levofloxacin; MINO, minocycline; NFLX, norfloxacin; RFP, rifampin; SM, streptomycin; PZFX, pazufloxacin.

nosis for distinguishing both *M. ulcerans* subsp. *shinshuense* and *M. ulcerans* infections from *M. marinum* infection. Although the DDH Mycobacteria kit could not distinguish *M. ulcerans* and *M. ulcerans* subsp. *shinshuense* from *M. marinum* (Table 5), simultaneous detection of IS*2404* would prevent misidentification. IS*2404* was well amplified from clinical samples and/or isolates in all 19 cases (Table 2). The 16S rRNA gene sequences of *M. ulcerans* subsp. *shinshuense* and *M. ulcerans* are similar, but conserved sites that were different in *M. ulcerans* subsp. *shinshuense* versus *M. ulcerans* were seen (Table 3); these matched perfectly with the sequences reported by Portaels et al. (20) and subsequently found to be useful in discrimination (6, 16). PCR targeting of pMUM001 revealed that all *M. ulcerans* subsp. *shinshuense* isolates lack the band representing the STPK gene, suggesting a small but conservative mutation(s) in *M. ulcerans* subsp. *shinshuense* versus *M. ulcerans* sequences. This PCR test was also applied for detection of a virulent plasmid and for differential diagnosis of *M. ulcerans* versus *M. ulcerans* subsp. *shinshuense* (16). The DNA sequence of the ITS region and the 16S rRNA and *hsp65* genes showed similarity between the *M. ulcerans* subsp. *shinshuense* isolates and *M. ulcerans*. However, the *rpoB* gene showed more similarity to *M. marinum* and *M. pseudoshottsii* than to *M. ulcerans* (Fig. 5). These data were suggestive of the evolutionary paths of these related mycobacterial species (9).

It is noteworthy that *M. ulcerans* subsp. *shinshuense* was identified in all of the isolates from Japanese patients diagnosed with BU. *M. ulcerans* subsp. *shinshuense*, not *M. ulcerans*, could be the primary etiological agent of BU in eastern Asia. It has been reported that the STPK gene was not amplified from the isolate of a BU patient in China (26). While there might be a taxonomical reason, this isolate was finally classified as *M. ulcerans* (4). A more precise genotypic examination might have revealed this to be a case of *M. ulcerans* subsp. *shinshuense* infection. If so, this finding would suggest that *M. ulcerans* subsp. *shinshuense* is distributed not only in Japan, but also in other areas of eastern Asia. Thorough field work and increased vigilance on the part of dermatologists and physicians are needed to determine the predominant cause of BU in eastern Asia. Because disease severity and susceptibility to antibacterial drugs are significantly different for *M. ulcerans* versus *M. ulcerans* subsp. *shinshuense*, they must be identified and distinguished in clinical settings.

The Japanese *M. ulcerans* subsp. *shinshuense* isolates and the Chinese strain of *M. ulcerans* presumably belong to the same cluster, based on genetic analyses such as microarray-based comparative genomic hybridization (9) and comparative sequence analysis of polymorphic variable-number tandem repeats (VNTR) (27). Their genomes were distinctly different from those of *M. ulcerans* strains that originated in other geographic regions. However, one of the VNTR loci can be used to distinguish between the Chinese and Japanese strains (1). Pidot et al. described the clear difference between the two strains by analyzing virulent plasmid genes and the resulting mycolactone production, noting that the Japanese strain produces mycolactone A/B, while the Chinese strain produces a unique mycolactone D (19). Further study is needed to elucidate the evolution and distribution of *M. ulcerans*, and its relation to *M. ulcerans* subsp. *shinshuense*, in Asia.

It is notable that most of the biochemical characteristics (Table 5) and drug susceptibilities (Table 6) of the isolates were the same as those found in a previous report (22), with the exception of the urease test. Interestingly, the Japanese *M. ulcerans* subsp. *shinshuense* isolates, the Chinese strain of *M. ulcerans*, and the related species *M. marinum* were all urease positive, though other strains of *M. ulcerans* originating from Ghana and Australia were urease negative. The urease test is a simple method with clear results that would be useful in distinguishing between *M. ulcerans* and *M. ulcerans* subsp. *shinshuense*.

Clinical manifestation of BU in Japan was essentially similar to that of BU in other countries, but distinct differences in management were observed. Ulcerated areas were usually smaller for Japanese (Fig. 3) than for African patients; how-

ever, the Japanese patients received both surgery and a large array of antimycobacterial drugs (Table 7). In addition, in Africa, most patients who had lesions with cross-sectional diameters of ≤10 cm showed excellent healing without surgery (17). Although the *in vitro* susceptibilities of the Japanese isolates to streptomycin, kanamycin, and clarithromycin are higher than those of the *M. ulcerans* strains from West Africa (Table 6), treatment has been fairly aggressive in Japan. It is speculated that because the majority of doctors and patients in Japan have not experienced and cannot recognize Buruli ulcer disease, they might fear the progression and recurrence of disease. Especially when patients complain of pain (9 patients in this study [47%] experienced pain [Fig. 4]), their doctors and family members are willing to initiate aggressive treatment, even in the absence of an immunodeficiency risk factor. Public information campaigns about the disease are needed, as is the establishment of guidelines for the treatment of Buruli ulcer in Japan. Clarification of the mode of transmission is also important. However, the occurrence of cases has been very sporadic, and none could be linked to an aquatic environment. Thus, the source and route of the infection remain unclear.

ACKNOWLEDGMENTS

This work was supported in part by a Grant-in-Aid for Research on Emerging and Re-emerging Infectious Diseases from the Ministry of Health, Labor, and Welfare of Japan (to Y.H., M.M., and N.I.), by a Grant-in-Aid for Scientific Research (C) from the Ministry of Education, Culture, Sports, Science and Technology of Japan (to Y.H.), and by a Grant-in-Aid for Scientific Research (C) from the Japan Society for the Promotion of Science (to K.N.).

REFERENCES

1. **Ablordey, A., et al.** 2005. Comparative nucleotide sequence analysis of polymorphic variable number tandem repeat loci in *Mycobacterium ulcerans*. J. Clin. Microbiol. **43**:5281–5284.
2. **Alsop, D. G.** 1972. The Bairnsdale ulcer. Aust. N. Z. J. Surg. **41**:317–319.
3. **Clancey, J. K., O. G. Dodge, H. F. Lunn, and M. L. Oduori.** 1961. Mycobacterial skin ulcers in Uganda. Lancet **ii**:951–954.
4. **Faber, W. R., et al.** 2000. First reported case of *Mycobacterium ulcerans* infection in a patient from China. Trans. R. Soc. Trop. Med. Hyg. **94**:277–279.
5. **Fenner, F.** 1951. The significance of the incubation period in infectious diseases. Med. J. Aust. **2**:813–818.
6. **Funakoshi, T., et al.** 2009. Intractable ulcer caused by *Mycobacterium shinshuense*: successful identification of mycobacterium strain by 16S ribosomal RNA 3′-end sequencing. Clin. Exp. Dermatol. **34**:e712–e715.
7. **Imada, H., et al.** 2008. Cutaneous ulcer of a right olecranon due to *Mycobacterium shinshuense*; a case report. Seikeigeka **59**:1440–1445. (In Japanese.)
8. **Kaminuma, E., et al.** 2010. DDBJ launches a new archive database with analytical tools for next-generation sequence data. Nucleic Acids Res. **38**(Database issue):D33–D38.
9. **Käser, M., et al.** 2007. Evolution of two distinct phylogenetic lineages of the emerging human pathogen *Mycobacterium ulcerans*. BMC Evol. Biol. **7**:177.
10. **Kazumi, Y., et al.** 2004. *Mycobacterium shinshuense* isolated from cutaneous ulcer lesion of right lower extremity in a 37-year-old woman. Kekkaku **79**:437–441. (In Japanese.)
11. **Kim, B.-J., et al.** 1999. Identification of mycobacterial species by comparative sequence analysis of the RNA polymerase gene (*rpoB*). J. Clin. Microbiol. **37**:1714–1720.
12. **Kondo, M., et al.** 2009. Leg ulcer caused by *Mycobacterium ulcerans* ssp. *shinshuense* infection. Int. J. Dermatol. **48**:1330–1333.
13. **Kusunoki, S., et al.** 1991. Application of colorimetric microdilution plate hybridization for rapid genetic identification of 22 *Mycobacterium* species. J. Clin. Microbiol. **29**:1596–1603.
14. **MacCallum, P., J. C. Tolhurst, G. Buckle, and H. I. Sissons.** 1948. A new mycobacterial infection in man. I. Clinical aspects. II. Experimental investigations in laboratory animals. III. Pathology of the experimental lesions in the rat. IV. Cultivation of the new mycobacterium. J. Pathol. Bacteriol. **60**:93–122.
15. **Mikoshiba, H., et al.** 1982. A case of atypical mycobacteriosis due to *Mycobacterium ulcerans*-like organism. Nihon Hifukagakkaizassi **92**:557–565. (In Japanese.)
16. **Nakanaga, K., et al.** 2007. "*Mycobacterium ulcerans* subsp. *shinshuense*" isolated from a skin ulcer lesion: identification based on 16S rRNA gene sequencing. J. Clin. Microbiol. **45**:3840–3843.
17. **Nienhuis, W. A., et al.** 2010. Antimicrobial treatment for early, limited *Mycobacterium ulcerans* infection: a randomized controlled trial. Lancet **375**: 664–672.
18. **Phillips, R. C., et al.** 2005. Sensitivity of PCR targeting the IS*2404* insertion sequence of *Mycobacterium ulcerans* in an assay using punch biopsy specimens for diagnosis of Buruli ulcer. J. Clin. Microbiol. **43**:3650–3656.
19. **Pidot, S. J., et al.** 2008. Deciphering the genetic basis for polyketide variation among mycobacteria producing mycolactones. BMC Genomics **9**:462.
20. **Portaels, F., et al.** 1996. Variability in 3′ end of 16S rRNA sequence of *Mycobacterium ulcerans* is related to geographic origin of isolates. J. Clin. Microbiol. **34**:962–965.
21. **Portaels, F., M. T. Silva, and W. M. Meyers.** 2009. Buruli ulcer. Clin. Dermatol. **27**:291–305.
22. **Portaels, F., P. Johnson, and W. M. Meyers (ed.).** April 2001. Buruli ulcer: diagnosis of *Mycobacterium ulcerans* disease. A manual for health care providers. World Health Organization, Geneva, Switzerland. http://whqlibdoc.who.int/hq/2001/WHO_CDS_CPE_GBUI_2001.4.pdf.
23. **Roth, A., et al.** 1998. Differentiation of phylogenetically related slowly growing mycobacteria based on 16S–23S rRNA gene internal transcribed spacer sequences. J. Clin. Microbiol. **36**:139–147.
24. **Springer, B., et al.** 1996. Isolation and characterization of a unique group of slowly growing mycobacteria: description of *Mycobacterium lentiflavum* sp. nov. J. Clin. Microbiol. **34**:1100–1107.
25. **Stinear, T. P., et al.** 2004. Giant plasmid-encoded polyketide synthases produce the macrolide toxin of *Mycobacterium ulcerans*. Proc. Natl. Acad. Sci. U. S. A. **101**:1345–1349.
26. **Stinear, T. P., et al.** 2005. Common evolutionary origin for the unstable virulence plasmid pMUM found in geographically diverse strains of *Mycobacterium* ulcerans. J. Bacteriol. **187**:1668–1676.
27. **Stragier, P., A. Ablordey, L. Durnez, and F. Portaels.** 2007. VNTR analysis differentiates *Mycobacterium ulcerans* and IS*2404* positive mycobacteria. Syst. Appl. Microbiol. **30**:525–530.
28. **Suzuki, S., et al.** 2008. Skin ulcer caused by '*Mycobacterium ulcerans* subsp. *shinshuense* ' infection. Hifubyou Shinryo **30**:145–148. (In Japanese.)
29. **Tamura, K., J. Dudley, M. Nei, and S. Kumar.** 2007. MEGA4: molecular evolutionary genetic analysis (MEGA) software version 4.0. Mol. Biol. Evol. **24**:1596–1599.
30. **Telenti, A., et al.** 1993. Rapid identification of mycobacteria to the species level by polymerase chain reaction and restriction enzyme analysis. J. Clin. Microbiol. **31**:175–178.
31. **Tsukamura, M., and H. Mikoshiba.** 1989. A taxonomic study on a mycobacterium which caused skin ulcer in a Japanese girl and resembled *Mycobacterium ulcerans*. Kekkaku **64**:691–697. (In Japanese.)
32. **Uganda Buruli Group.** 1971. Epidemiology of *Mycobacterium ulcerans* infection (Buruli ulcer) at Kinyara, Uganda. Trans. R. Soc. Trop. Med. Hyg. **65**:763–775.
33. **Wallace, R. J., Jr, D. R. Nash, L. C. Steele, and V. Steingrube.** 1986. Susceptibility testing of slowly growing mycobacteria by a microdilution MIC method with 7H9 broth. J. Clin. Microbiol. **24**:976–981.
34. **Walsh, D. S., F. Portaels, and W. M. Meyers.** 2011. Buruli ulcer: advances in understanding *Mycobacterium ulcerans* infection. Dermatol. Clin. **29**:1–8.
35. **Watanabe, T., et al.** 2010. Buruli ulcer caused by "*Mycobacterium ulcerans* subsp. *shinshuense*." Eur. J. Dermatol. **20**:809–810.
36. **World Health Organization.** October 2004. Provisional guidance on the role of specific antibiotics in the management of *Mycobacterium ulcerans* disease (Buruli ulcer). World Health Organization, Geneva, Switzerland. http://whqlibdoc.who.int/hq/2004/WHO_CD5_CPE_GBUI_2004.10.pdf..

JOURNAL OF BACTERIOLOGY, Oct. 2011, p. 5766–5774 Vol. 193, No. 20
0021-9193/11/$12.00 doi:10.1128/JB.05412-11

Structure and Host Recognition of Serotype 13 Glycopeptidolipid from *Mycobacterium intracellulare*▽†

Takashi Naka,[1,2]‡ Noboru Nakata,[3]‡ Shinji Maeda,[4]‡ Reina Yamamoto,[1,5] Matsumi Doe,[6] Seiko Mizuno,[1,5] Mamiko Niki,[1] Kazuo Kobayashi,[7] Hisashi Ogura,[1,8] Masahiko Makino,[3] and Nagatoshi Fujiwara[1]*

Departments of Bacteriology[1] and Virology,[8] Osaka City University Graduate School of Medicine, Osaka 545-8585, Japan; MBR Co. Ltd., Osaka 560-8552, Japan[2]; Department of Mycobacteriology, Leprosy Research Center, National Institute of Infectious Diseases, Tokyo 189-0002, Japan[3]; Molecular Epidemiology Division, Mycobacterium Reference Center, The Research Institute of Tuberculosis, Japan Anti-Tuberculosis Association, Tokyo 204-8533, Japan[4]; Department of Development Nourishment, Faculty of Human Development, Soai University, Osaka 559-0003, Japan[5]; Department of Chemistry, Graduate School of Science, Osaka City University, Osaka 558-8585, Japan[6]; and Department of Immunology, National Institute of Infectious Diseases, Tokyo 162-8640, Japan[7]

Received 31 May 2011/Accepted 31 July 2011

The *Mycobacterium avium-M. intracellulare* complex (MAIC) is divided into 28 serotypes by a species-specific glycopeptidolipid (GPL). Previously, we clarified the structures of serotype 7 GPL and two methyltransferase genes (*orfA* and *orfB*) in serotype 12 GPL. This study elucidated the chemical structure, biosynthesis gene, and host innate immune response of serotype 13 GPL. The oligosaccharide (OSE) structure of serotype 13 GPL was determined to be 4-2′-hydroxypropanoyl-amido-4,6-dideoxy-β-hexose-(1→3)-4-*O*-methyl-α-L-rhamnose-(1→3)-α-L-rhamnose-(1→3)-α-L-rhamnose-(1→2)-α-L-6-deoxy-talose by using chromatography, mass spectrometry, and nuclear magnetic resonance (NMR) analyses. The structure of the serotype 13 GPL was different from those of serotype 7 and 12 GPLs only in *O*-methylations. We found a relationship between the structure and biosynthesis gene cluster. *M. intracellulare* serotypes 12 and 13 have a 1.95-kb *orfA-orfB* gene responsible for 3-*O*-methylation at the terminal hexose, *orfB*, and 4-*O*-methylation at the rhamnose next to the terminal hexose, *orfA*. The serotype 13 *orfB* had a nonfunctional one-base missense mutation that modifies serotype 12 GPL to serotype 13 GPL. Moreover, the native serotype 13 GPL was multiacetylated and recognized via Toll-like receptor 2. The findings presented here imply that serotypes 7, 12, and 13 are phylogenetically related and confirm that acetylation of the GPL is necessary for host recognition. This study will promote better understanding of the structure-function relationships of GPLs and may open a new avenue for the prevention of MAIC infections.

The increase of drug-resistant mycobacteria and the number of immunocompromised hosts including the HIV epidemic are important problems. The *Mycobacterium avium-M. intracellulare* complex (MAIC) is distributed ubiquitously in the environment and is the most common isolate of nontuberculous mycobacteria, which are now one of the most important environmental pathogen-disseminated infectious agents in both immunocompromised and immunocompetent hosts (26, 31, 39).

The most characteristic feature of mycobacteria is richness in lipids. These hydrophobic cell wall components contribute to the surface properties and are considered to play important roles in their pathogenesis through the host immune responses (8, 17). MAIC expresses a glycopeptidolipid (GPL) as one of the representative lipid components. Structurally, the GPL is composed of two parts, a common tetrapeptido-amino alcohol core and a serotype-specific oligosaccharide (OSE) elongated from 6-deoxy-talose (6-d-Tal). D-Phenylalanine-D-*allo*-threonine-D-alanine-L-alaninol (D-Phe-D-*allo*-Thr-D-Ala-L-alaninol), which is modified with an amido-linked 3-hydroxy or 3-methoxy C_{26}-C_{34} fatty acid at the *N* terminus of D-Phe, and D-*allo*-Thr and terminal L-alaninol are further linked to a 6-d-Tal and 3,4-di-*O*-methyl rhamnose (3,4-di-*O*-Me-Rha), respectively. This portion is called the serotype-nonspecific GPL (apolar GPL). Serotype-specific GPLs (polar GPLs) are produced by extending individual OSE residues from the 6-d-Tal. MAIC species are divided into 28 serotypes by serological reaction and distinctive patterns of polar GPLs on thin-layer chromatography (TLC) (7, 38). The GPL is considered to play crucial roles in the physiology of the bacteria and the host responses to MAIC infection. Several biological and immunological functions of GPLs have been reported (9, 34), but the roles of GPLs are not fully elucidated. Recently, several genes involved in GPL biosynthesis have been characterized (10, 29). To better understand the biological functions and significance of GPLs, we need to clarify the structure and biosynthetic pathways of GPLs.

The chemical structures of only 16 GPLs have been defined (9). Recently, we determined the structures of the serotype 7 and 16 GPLs and identified the gene clusters completing the OSE biosynthesis (13, 14). In addition, two methyltransferase genes of serotype 7- and 12-specific GPL biosynthesis were

* Corresponding author. Mailing address: Department of Bacteriology, Osaka City University Graduate School of Medicine, 1-4-3 Asahi-machi, Abeno-ku, Osaka 545-8585, Japan. Phone: 81 6 6645 3746. Fax: 81 6 6645 3747. E-mail: fujiwara@med.osaka-cu.ac.jp.

† Supplemental material for this article may be found at http://jb.asm.org/.

‡ These authors contributed equally to this work.

▽ Published ahead of print on 19 August 2011.

characterized (30). In this process, we found that the structure of the serotype 13 GPL is close to that of the serotype 7 and 12 GPLs. In epidemiological serotyping, Tsang et al. (37) showed that clinical isolates of serotypes 7, 12, and 13 were found in around 10% of non-AIDS patients. However, it was difficult to distinguish serotypes 7, 12, and 13 by only serological and chromatographic techniques because of their structural similarity. The phylogeny of some MAIC strains based on GPL biosynthesis genes has been reported (23). In this study, the complete structure of the serotype 13 GPL was determined, and the genetic relationship between the serotype 7, 12, and 13 GPL biosynthesis was clarified. Moreover, the host innate immune recognition of antigenic serotype 13 GPL and the importance of structural modification were shown. We discuss the phylogeny of MAIC strains on the basis of these GPL biosynthesis genes and the relationship between GPL structure and immunogenicity.

MATERIALS AND METHODS

Bacterial strains and preparation of GPL. *M. intracellulare* serotype 13 (ATCC 35769, ATCC 25122), serotype 7 (ATCC 35847), and serotype 12 (ATCC 35762) strains were purchased from the American Type Culture Collection (Manassas, VA). The GPL preparation was performed as described previously (14, 18). Each strain of *M. intracellulare* was grown on Middlebrook 7H11 agar (Difco Laboratories, Detroit, MI) with 0.5% glycerol and 10% Middlebrook oleic acid-albumin-dextrose-catalase (OADC) enrichment (Difco) at 37°C for 2 to 3 weeks. The heat-killed bacteria were sonicated, and crude lipids were extracted with chloroform-methanol (2:1 [vol/vol]). The crude lipids were hydrolyzed with 0.2 N sodium hydroxide in methanol at 37°C for 2 h, followed by neutralization with 6 N hydrochloric acid. Alkaline-stable lipids were partitioned by a two-layer system with chloroform-methanol (2:1 [vol/vol]) and water. The organic phase was evaporated and precipitated with acetone to remove any acetone-insoluble components. The supernatant was washed (chloroform-methanol, 95:5 [vol/vol]) and eluted (chloroform-methanol, 1:1 [vol/vol]) with a Sep-Pak silica cartridge (Waters Corporation, Milford, MA) for partial purification. The GPL was completely purified by preparative TLC of Silicagel G (Uniplate; 20 by 20 cm, 250 μm; Analtech, Inc., Newark, DE). The TLC plate was developed with chloroform-methanol-water (65:25:4 and 60:16:2 [vol/vol/vol]), until a single spot was obtained. The TLC plate was sprayed with 20% sulfuric acid in ethanol and was charred at 180°C for 3 min. The GPL was detected as a brownish-yellow spot. To recover the GPL, the TLC plate was exposed to iodine vapor, and the GPL spot was marked. The silica gels of the GPL spot were scraped off, and the GPL was eluted with chloroform-methanol (2:1 [vol/vol]). The native GPL was purified by the same method as the alkaline-stable GPL, omitting the hydrolysis with 0.2 N sodium hydroxide.

Preparation of OSE moiety. β-Elimination of the GPL was performed with alkaline borohydride, and the OSE elongated from D-*allo*-Thr was released (14, 18). The GPL was stirred in a solution of equal volumes of ethanol and 10 mg/ml sodium borodeuteride in 0.5 N sodium hydroxide at 60°C for 16 h. The reaction mixture was decationized with Dowex 50W X8 beads (Dow Chemical Company, Midland, MI) and evaporated under nitrogen to remove boric acid. After partition into two layers of chloroform-methanol (2:1 [vol/vol]) and water, the upper aqueous phase was recovered and evaporated, and the OSE was purified as an oligoglycosyl alditol.

MALDI-TOF MS and MALDI-TOF MS/MS. The molecular species of the intact GPL was determined by the matrix-assisted laser desorption ionization–time of flight mass spectrometry (MALDI-TOF MS) with an Ultraflex II (Bruker Daltonics, Billerica, MA). One microgram of the GPL-dissolved chloroform-methanol (2:1 [vol/vol]) was applied to the target plate, and 1 μl of 10 mg/ml 2,5-dihydroxybenzoic acid in chloroform-methanol (1:1 [vol/vol]) was added as a matrix. The intact GPL was analyzed in the Reflectron mode with an accelerating voltage operating in positive mode at 20 kV (4). Then, the fragment pattern of the OSE was analyzed with the MALDI-TOF MS/MS mode. The OSE and 10 mg/ml 2,5-dihydroxybenzoic acid was dissolved in ethanol-water (3:7 [vol/vol]) and applied to the target plate according to the method for intact GPL.

GC/MS of carbohydrates. To determine the glycosyl composition and linkage position, gas chromatography/mass spectrometry (GC/MS) of partially methylated alditol acetate derivatives was performed. Perdeuteromethylation was conducted by the modified procedure of Hakomori (14, 15). The OSE was dissolved with a mixture of dimethyl sulfoxide and sodium hydroxide, followed by the addition of deuteromethyl iodide. After stirring at room temperature for 15 min, the reaction mixture was separated by a two-layer system of water and chloroform. The chloroform-containing perdeuteromethylated OSE layer was collected, washed with water two times, and evaporated completely. Partially deuteromethylated alditol acetate derivatives were prepared from perdeuteromethylated OSE by hydrolysis with 2 N trifluoroacetic acid at 120°C for 2 h, reduction with 10 mg/ml sodium borodeuteride at 25°C for 2 h, and acetylation with acetic anhydride at 100°C for 1 h (14, 19). GC/MS was performed using a benchtop ion trap mass spectrometer (GCMS-QP2010 Plus; Shimadzu Corp., Kyoto, Japan) equipped with a fused capillary column (SP-2380 and Equity-1; 30 m, 0.25-mm inner diameter [ID]; Supelco, Bellefonte, PA). Helium was used

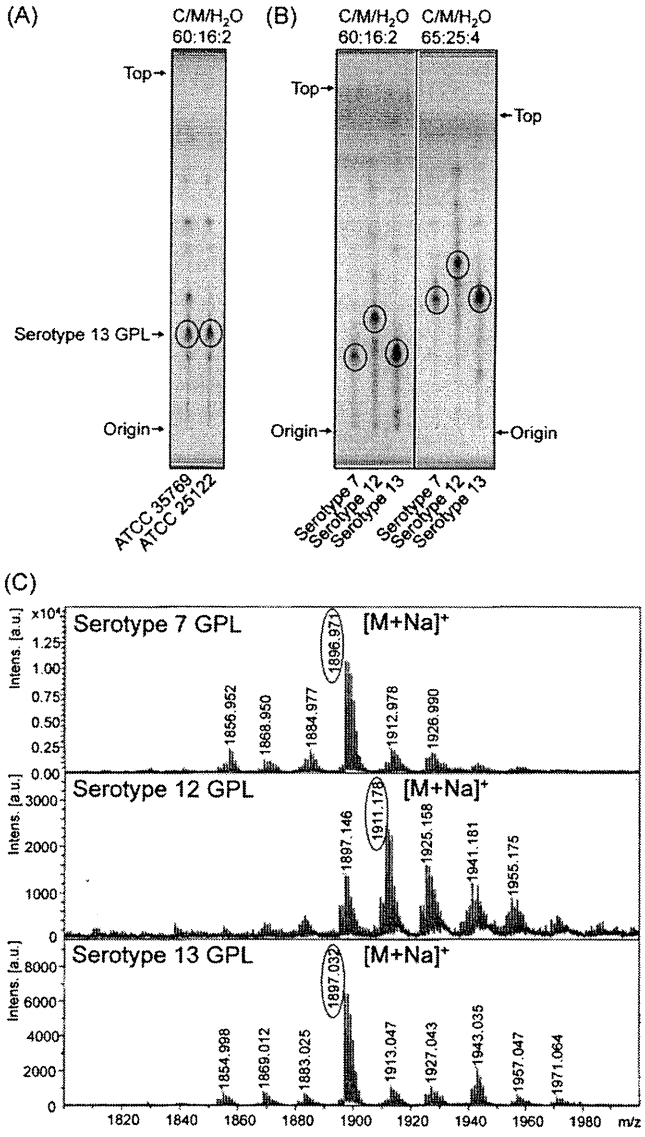

FIG. 1. TLC patterns and MALDI-TOF MS spectra of serotype 7, 12, and 13 GPLs. (A and B) The alkaline-stable lipids derived from *M. intracellulare* serotype 13 ATCC 35769 and ATCC 25122 (A) and the purified serotype 7, 12, and 13 GPLs (B) were developed on TLC plates with solvent systems of chloroform-methanol-water (60:16:2 and 65:25:4 [vol/vol/vol]). (C) The MALDI-TOF MS spectra of serotype 7, 12, and 13 GPLs were acquired using 10 mg/ml 2,5-dihydroxybenzoic acid in chloroform-methanol (1:1 [vol/vol]) as a matrix, and the molecular ions were detected as $[M+Na]^+$ in positive mode. Intens., intensity; a.u., arbitrary units.

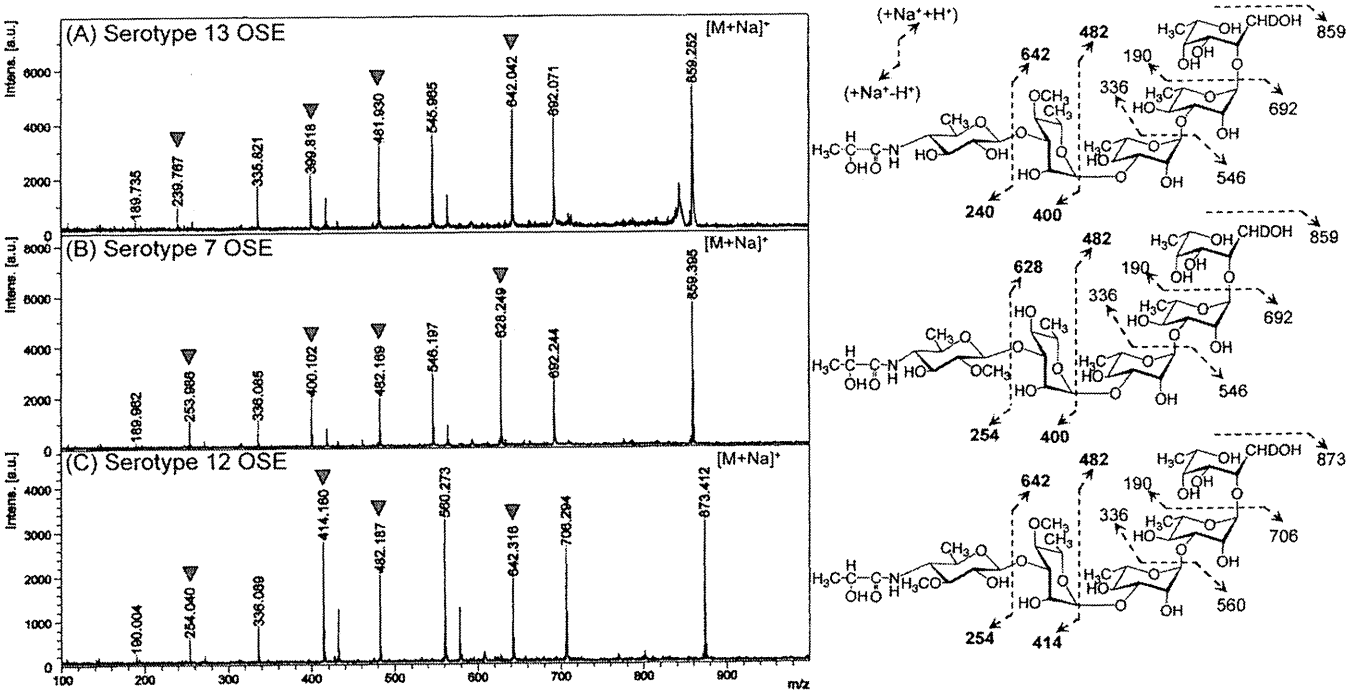

FIG. 2. MALDI-TOF MS/MS spectra of serotype 13, 7, and 12 OSEs (A, B, and C, respectively). The fragment ions by each glycosyl cleavage were detected, and the assigned fragment patterns are illustrated. Arrowheads indicate the characteristic mass numbers of the serotype 13, 7, and 12 OSEs. The matrix was 10 mg/ml 2,5-dihydroxybenzoic acid in ethanol-water (3:7 [vol/vol]), and it was performed in the MS/MS mode. Intens., intensity; a.u., arbitrary units.

as the carrier gas, and the flow rate was 1 ml/min. The temperature program for alditol acetate derivatives was started at 60°C, increased 40°C/min to 220°C, and held for 15 min, followed by an increase of 10°C/min to 260°C and holding for 10 min. The molecular separator and ion source energies were 70 eV, and the accelerating voltage was 8 kV.

NMR of GPL. The OSE was dissolved in deuterium oxide. To define the anomeric configurations of each glycosyl residue, ^{1}H and ^{13}C nuclear magnetic resonance (NMR) was employed. Both homonuclear correlation spectrometry (COSY) and ^{1}H-detected [^{1}H, ^{13}C] heteronuclear multiple-quantum correlation (HMQC) were recorded with a Bruker AVANCE-600 (Bruker BioSpin Corp. Billerica, MA), as described previously (14, 18). Ten microliters of acetone was added to the sample, and its chemical shift values, 2.04 ppm (proton) and 29.8 ppm (carbon), were used as internal controls.

Sequencing of *orfA-orfB* region of *M. intracellulare* serotype 13. PCR was used to amplify the *orfA-orfB* region (30) of *M. intracellulare* serotype 13 (ATCC 35769 and ATCC 25122), using primers *orfA*-F (5′-GCGGATCCAGTGTGCAGACG AGCGGAACT-3′), *orfA*-R (5′-GCGAATTCTTATCGAGAAAAAATAAAA G-3′), *orfB*-F (5′-GCGGATCCACTGCTAGACT CCGCCACCAT-3′), and *orfB*-R (5′-GCGAATTCCTACACCTTCACGGCGAGTC-3′). The amplified fragment was sequenced using a BigDye Terminator cycle sequencing kit, version 3.1 (Applied Biosystems, Foster City, CA), and a sequence analyzer (ABI3130xl; Applied Biosystems).

Transformation of *M. intracellulare* serotype 13 strain with serotype 12 *orfB*. The *orfB* fragments from serotype 12 (sero12-*orfB*) and serotype 13 (sero13-*orfB*) strains were amplified and cloned into pVV16, an expression plasmid vector for mycobacteria, downstream of the hsp60 promoter. *M. intracellulare* serotype 13 ATCC 35769 was transformed with pVV16-sero12-*orfB* and pVV16-sero13-*orfB* by electroporation, and hygromycin- and kanamycin-resistant colonies were isolated. Alkaline-stable lipids were prepared from heat-killed bacteria, and productive GPLs were identified by TLC, MALDI-TOF MS, MALDI-TOF MS/MS, and GC/MS.

Host recognition of native and alkaline-treated serotype 13 GPLs. The host recognition of GPLs was estimated by activations of HEK-blue-2 and -4 cells (InvivoGen, San Diego, CA). HEK-blue-2 and -4 cells are HEK293 cells stably transfected with multiple genes for recognition of Toll-like receptor 2 (TLR2) and TLR4 (including the coreceptors MD2 and CD14). In addition, HEK-blue-2 and -4 cells stably express an optimized alkaline phosphatase gene engineered to be secreted (sAP) and placed under the control of a promoter inducible by several transcription factors, such as NF-κB and alkaline phosphatase-1. HEK-blue-2 and -4 cells were seeded at a concentration of 2×10^5 cells/ml in 96-well flat-bottom tissue culture plates and incubated with Dulbecco's modified Eagle's medium (DMEM) containing 10% fetal bovine serum (FBS) at 37°C in an atmosphere of 5% CO_2 for 3 days. The adherent HEK-blue-2 and -4 cells were stimulated by native and alkaline-treated serotype 13 GPLs. After 24 h of incubation, NF-κB activation was assayed by the levels of sAP in the supernatant. The sAP was measured in duplicate using QUANTI-Blue (InvivoGen) according to the manufacturer's instructions. As positive controls, we used lipopolysaccharide (LPS) from *Escherichia coli* 055:B5 (Sigma-Aldrich, St. Louis, MO) for TLR4 and Pam3CSK4 (InvivoGen) for TLR2. Two independent experiments were performed.

Nucleotide sequence accession number. The nucleotide sequence reported here has been deposited in the NCBI GenBank database under accession number AB557690.

RESULTS

Purification and molecular weight of intact GPL. The serotype 13 GPLs from *M. intracellulare* ATCC 35769 and 25122 were detected as spots on TLC plates and showed the same R_f value (Fig. 1A). Because serotype 13 GPL was predicted to be very close structurally to the serotype 7 and 12 GPLs, the R_f values were compared on TLC plates developed with two different chloroform-methanol-water solvent systems (65:25:4 and 60:16:2 [vol/vol/vol]), respectively. Interestingly, the R_f value of the serotype 13 GPL was lower than that of the serotype 12 GPL and almost the same as that of the serotype 7 GPL in both developing systems (Fig. 1B). The intact molecular weight of each GPL was determined. The MALDI-TOF MS spectrum of the serotype 13 GPL showed *m/z* 1,897 for $[M+Na]^+$ as the main molecular ion in positive mode (Fig.

1C). This mass number is identical to that of the serotype 7 GPL ($[M+Na]^+$: 1,897) and 14 atomic mass units lower than that of the serotype 12 GPL ($[M+Na]^+$: 1,911).

Glycosyl sequence of serotype 13 OSE. To determine the glycosyl sequence of the OSE, MALDI-TOF MS/MS of the oligoglycosyl alditol from serotype 13 OSE was performed. The spectrum afforded the molecular ion $[M+Na]^+$ at *m/z* 859, together with the characteristic mass increments in the series of glycosyloxonium ions formed on fragmentation at *m/z* 240, 400, 546, and 692 from the *N*-acylated Hex to 6-d-Tal, and at *m/z* 190, 336, 482, and 642 from 6-d-Tal to *N*-acylated Hex (Fig. 2A). In comparison, the fragment patterns of the cleaved terminal *N*-acylated Hex of the OSEs were *m/z* 254 and 628 in serotype 7 and *m/z* 254 and 642 in serotype 12, and those next to the terminal Hex were *m/z* 400 and 482 in serotype 7 and *m/z* 414 and 482 in serotype 12 (Fig. 2B and C). Together with the intact molecular weight of each GPL (Fig. 1B), these results strongly implied that serotype 13 GPL has no *O*-methyl group in the terminal *N*-acylated Hex but does have an *O*-methyl group added to the Rha next to the terminal Hex.

Carbohydrate composition and linkage analyses. GC/MS analysis of the perdeuteromethylated alditol acetate derivative from serotype 13 OSE was performed to determine the glycosyl composition. The total ion chromatography (TIC) of the GC/MS spectrum of serotype 13 GPL derivatives was compared to those of serotype 7 and 12 GPL derivatives (Fig. 3A). Previous reports showed that the carbohydrate compositions of the serotype 7 GPL were 6-d-Tal, Rha, and 4-2′-hydroxypropanoyl-amido-3,6-dideoxy-2-*O*-Me-Hex, and those of the serotype 12 GPL were 6-d-Tal, Rha, 4-*O*-Me-Rha, and 4-2′-hydroxypropanoyl-amido-3,6-dideoxy-3-*O*-Me-Hex (5, 13). Comparison of the retention times and mass spectra of GC/MS determined that serotype 13 GPL was composed of 6-d-Tal, Rha, 4-*O*-Me-Rha, and another terminal *N*-acylated Hex. As shown in Fig. 3B, the perdeuteromethylated alditol acetate derivative of the terminal *N*-acylated Hex was assigned to 2,3-di-*O*-deuteromethyl-1,5-di-*O*-acetyl-4-2′-*O*-deuteromethyl-propanoyl-deuteromethylamido-4,6-dideoxy-hexitol from the fragment pattern (*m/z* 62, 108, 121, 168, 209, 222, 269, and 303). These results confirmed that the *O*-methyl group was deleted from the terminal *N*-acylated Hex and added to the C-4 position at Rha next to the terminal Hex. Taken together, these results established the sequence and linkage arrangement of 4-2′-hydroxypropanoyl-amido-4,6-dideoxy-Hex-(1→3)-4-*O*-Me-Rha-(1→3)-L-Rha-(1→3)-L-Rha-(1→2)-6-d-Tal exclusively.

NMR analysis of serotype 13 OSE. The ^1H NMR and ^1H-^1H homonuclear COSY analyses of the OSE derived from the serotype 13 GPL revealed four distinct anomeric protons with corresponding H1-H2 cross-peaks in the low-field region at δ4.88, 4.71, 4.97 (J_{1-2} = 1 to 2 Hz, indicative of α-anomers), and 4.52 (a doublet, J_{1-2} = 7.9 Hz, indicative of a β-hexosyl unit). When further analyzed by ^1H-detected [^1H-^{13}C] two-dimensional HMQC, the anomeric protons resonating at δ4.88, 4.71, 4.97, and 4.52 had C-1s resonating at δ102.10, 93.50, 94.00, and 103.40, respectively. The J_{CH} values for each of these protons were calculated to be 170, 170, 171, and 161 Hz by measurement of the inverse-detection nondecoupled two-dimensional HMQC (see Fig. S1 and Table S1 in the supplemental material). It was concluded that two Rha and 4-*O*-Me Rha were α-anomers and that the terminal *N*-acylated Hex was a β configuration.

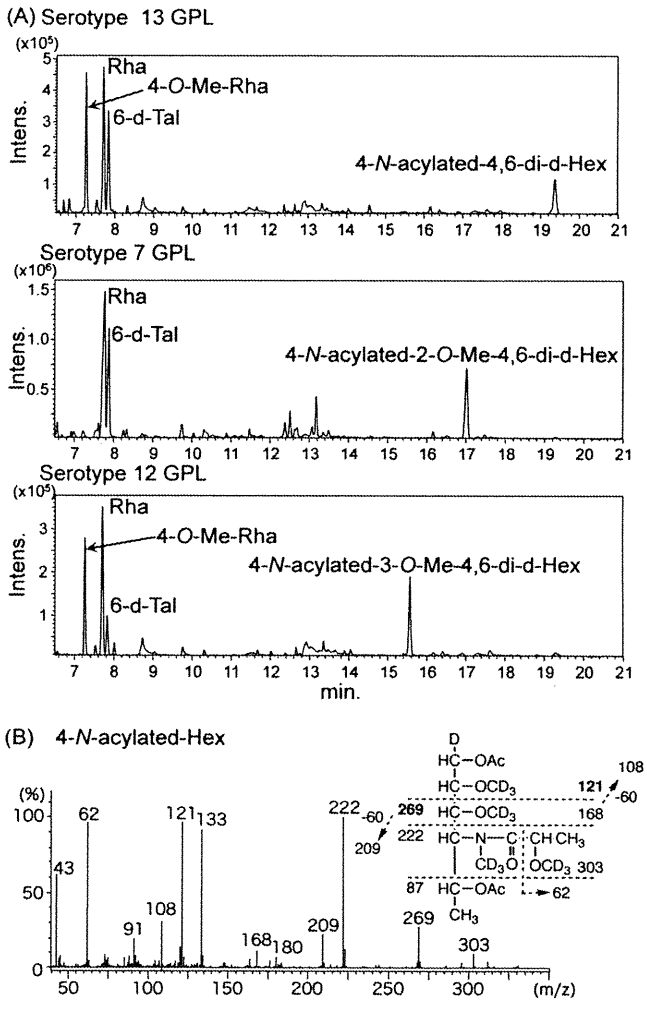

FIG. 3. Assignment of glycosyl composition of OSEs in serotype 13 GPL. (A) Total ion chromatogram of the alditol acetate derivatives from serotype 13 compared to those of serotype 7 and 12 GPLs. A fused SP-2380 capillary column was used as the GC column. The temperature program for alditol acetate derivatives was started at 60°C, increased to 40°C/min to 220°C, and held for 15 min, followed by an increase of 10°C/min to 260°C and holding for 10 min. (B) GC/MS spectrum of the perdeuteromethylated alditol acetate derivative from the terminal Hex in serotype 13 GPL. The pattern of prominent fragment ions is illustrated. A fused Equity-1 capillary column was used as the GC column. Ac, CH_3CO.

Nucleotide sequence of *orfA-orfB* region of *M. intracellulare* serotype 13. The present study demonstrated that the difference between the chemical structures of the serotype 13 GPL and serotype 7 and 12 GPLs was whether the *O*-methyl group in the terminal *N*-acylated Hex and the next Rha were present or not. We confirmed the genetic basis of these *O*-methylations. Our previous study clarified three unique open reading frames (ORFs) for methyltransferase, named *orf2*, derived from *M. intracellulare* serotype 7, and *orfA* and *orfB*, from *M. intracellulare* serotype 12 (13, 30). *orfA* and *orfB* in *M. intracellulare* serotype 12 are responsible for 4-*O*-methylation of the Rha next to the terminal Hex and 3-*O*-methylation of the

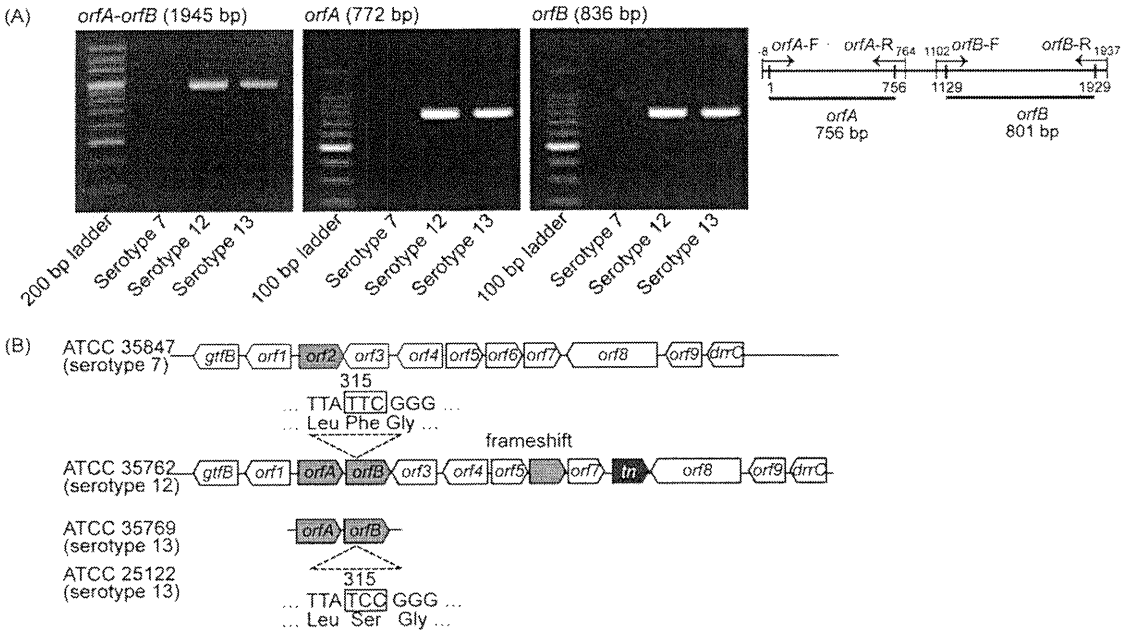

FIG. 4. Detection of *orfA-orfB* regions and comparison of genetic maps of GPL biosynthetic cluster. (A) PCR was performed to amplify the *orfA-orfB* regions of *M. intracellulare* serotype 7, 12, and 13 strains. The primers and the amplified regions are indicated. (B) *M. intracellulare* serotype 7 ATCC 35847 and serotype 12 ATCC 35762 were sequenced in our previous work (13, 30). *M. intracellulare* serotype 13 ATCC 35769 and ATCC 25122 were sequenced in this study. The missense mutation of *orfA-orfB* regions is indicated.

terminal Hex, respectively. Therefore, we examined whether or not *M. intracellulare* serotype 13 has these ORFs. First, comparison of the *gtfB-drrC* gene cluster in *M. intracellulare* serotype 7 and 12 strains implied that *orf2* in *M. intracellulare* serotype 7 replaced *orfA-orfB* in *M. intracellulare* serotype 12. We amplified the *orfA-orfB* in the genomic DNA from *M. intracellulare* serotypes 7, 12, and 13 (Fig. 4A). Interestingly, *M. intracellulare* serotype 13 had the same-sized DNA fragment of the *orfA-orfB* region, and the nucleotide sequences were determined. The 1.95-kb *orfA-orfB* regions of the two serotype 13 strains had complete identity and showed only one nucleotide substitution from that of serotype 12: codon 105, TTC, of the *orfB* in serotype 12 was replaced by codon TCC in serotype 13 (Fig. 4B). This missense mutation induced a single amino acid substitution from Phe to Ser and implied the loss of the *orfB* activity for *O*-methylation.

Expression of sero12-*orfB* and sero13-*orfB* in *M. intracellulare* serotype 13. To test the functional activity of *orfB* in *M. intracellulare* serotypes 12 and 13, the sero12-*orfB* and sero13-*orfB* genes were introduced into the *M. intracellulare* serotype 13 strain. The 0.84-kb sero12-*orfB* and sero13-*orfB* were amplified and cloned into a pVV16 vector, and *M. intracellulare* serotype 13 ATCC 35769 was transformed with the resulting plasmids and the pVV16 vector. The alkaline-stable lipids derived from the transformants were developed on TLC plates, and the productive GPLs were compared to the spots of serotype 7, 12, and 13 GPLs (Fig. 5A). Both R_f values of the GPLs produced in the transformants with the pVV16 vector and sero13-*orfB* were identical to that of the serotype 13 GPL. However, the R_f value of the GPL produced in the transformant with sero12-*orfB* was the same as that of serotype 12 GPL. By MALDI-TOF MS, the main molecular weights of the GPLs produced in the transformants with sero12-*orfB*, sero13-*orfB*, and the pVV16 vector were detected as *m/z* 1,911, 1,897, and 1,897, respectively, for $[M+Na]^+$ (data not shown). The fragment ions of the related glycosyl cleavage in the OSEs were analyzed by using MALDI-TOF MS/MS, and the glycosyl compositions were determined. The fragment ions of the OSEs in the pVV16 vector and sero13-*orfB* showed the same pattern as serotype 13 GPL, indicating that overexpression of sero13-*orfB* in the serotype 13 strain was not affected (Fig. 2A and 5B). The fragment ions of the OSE in sero12-*orfB*, i.e., *m/z* 254 and 414, were different from those of the OSE in sero13-*orfB*, i.e., *m/z* 240 and 400, respectively (Fig. 5B). The GC/MS spectrum of the perdeuteromethylated alditol acetate derivative of the terminal *N*-acylated Hex from sero12-*orfB* was assigned to 2-*O*-deuteromethyl-1,5-di-*O*-acetyl-4-2′-*O*-deuteromethyl-propanoyl-deuteromethylamido-4,6-dideoxy-3-*O*-methyl-hexitol from the fragment pattern (*m/z* 62, 105, 121, 165, 206, 222, 266, and 300) (Fig. 5C), which was identical to that of the serotype 12 GPL. These results demonstrated that the serotype 13 transformant with sero12-*orfB* but not sero13-*orfB* had an added *O*-methyl group at the C-3 position in the terminal Hex and that the productive GPL was completely changed from serotype 13 to serotype 12. In addition, we confirmed that the plasmid-deleted C-terminal 40-base region of sero12-*orfB* was completely functional and that sero12-*orfB* worked in the serotype 7 transformant. Taken together, these results indicated that sero13-*orfB* was inactivated by the missense mutation at codon 105 and that the serotype 13 GPL lacked *O*-methylation at the C-3 position of the terminal Hex.

Native conformation of serotype 13 GPL and host response. The native serotype 13 GPL was purified without alkaline treatment. The native serotype 13 GPLs were detected on TLC

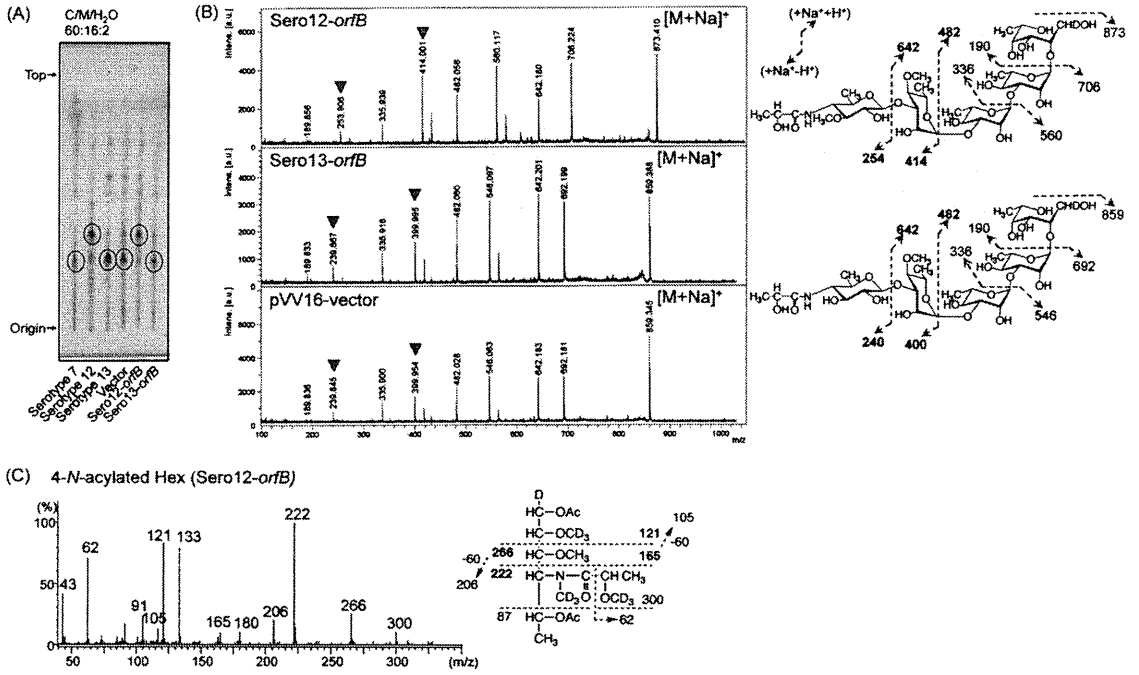

FIG. 5. The productive GPLs in transformants of *M. intracellulare* serotype 13 with sero12-*orfB* or sero13-*orfB*. (A) TLC patterns of the alkaline-stable lipids derived from *M. intracellulare* serotypes 7, 12, and 13 and serotype 13 transformants (ATCC 35769) with the pVV16-vector, sero12-*orfB*, and sero13-*orfB* from left to right, developing with a solvent system of chloroform-methanol-water (60:16:2 [vol/vol/vol]). (B) MALDI-TOF MS/MS spectra of OSEs derived from the productive GPLs in transformants of *M. intracellulare* serotype 13 with sero12-*orfB*, sero13-*orfB*, and the pVV16 vector. The replaced mass numbers are indicated by arrowheads. (C) GC/MS spectrum of the perdeuteromethylated alditol acetate derivative of the terminal *N*-acylated Hex from serotype 13 transformant with sero12-*orfB*. The MALDI TOF MS/MS and GC/MS conditions are described in the legends for Fig. 2 and 3. Ac, CH_3CO.

plates as three major spots that expanded broadly and had R_f values different from that of the alkaline-treated serotype 13 GPL. These spots were converged into one spot by alkaline treatment (Fig. 6A). It was reported that some positions of OSE in GPLs are acetylated in nature (27). The molecular weights of these three spots were checked by MALDI-TOF MS. The mass numbers of *m/z* 1,983, 2,025, and 2,067 for $[M+Na]^+$ caused the 2- to 4-unit increases of *m/z* 42 (addition of acetylations) and the modification to saturated alkyl group, compared to *m/z* 1,897 of the alkaline-treated serotype 13 GPL, implying that native GPLs were modified by several *O*-acetylations in the OSE portion and that alkaline treatment removed the acetylated groups (Fig. 6B). In addition, several peaks at intervals of 14 atomic mass units were caused by an alkyl group, indicating that the fatty acids of the core portion were variable and that the molecular species were heterogeneous.

To clarify the host recognitions of serotype 13 GPL via TLRs, we stimulated HEK-blue-2 and -4 cells with native and alkaline-treated serotype 13 GPLs. The native serotype 13 GPL significantly activated HEK-blue-2 cells in a dose-dependent manner, but HEK-blue-4 cells did not respond. The alkaline-treated serotype 13 GPL without *O*-acetylation did not activate either HEK-blue-2 or -4 cells. Reacetylated alkaline-treated serotype 13 GPLs with *O*-acetyl groups substituted for all hydroxy groups of OSE activated HEK-blue-2 cells, although the level of activation was less than that of the native form (Fig. 6C). Moreover, we confirmed that only the native serotype 13 GPL stimulated mouse bone marrow-derived macrophages via TLR2 by using C57BL/6 and TLR2 knockout mice (see Fig. S2 in the supplemental material).

DISCUSSION

The structural heterogeneity of the GPLs in MAIC species is reflected in their morphology, virulence, and pathogenicity (2, 3, 24) and may be meaningful in phylogenetic classification. Actually, epidemiological studies show that the isolates of MAIC serotypes from patients are heterogeneous and important for assessing the prognosis of pulmonary MAIC disease (25, 37). Chatterjee and Khoo (9) proposed grouping the three types of GPLs by OSE structure, and the group 2 GPLs included the serotype 12, 17, and 19 strains. The serotype 7 and 16 GPLs determined in our previous studies also belong to the group 2 GPLs (13, 14). The group 2 GPLs have in common 6-d-Tal-Rha-Rha and serotype-individual sugars elongated from the second Rha. In addition, except for the serotype 19 GPL, group 2 GPLs carry an unusual substituent, *N*-acylated amido sugar, as the terminal Hex. Aspinall et al. (1) mentioned that the terminal sugar residue of serotype 12 GPL is a derivative of viosamine (4-amino-4,6-dideoxyglucose). The structural difference between serotype 7 and 12 GPLs in group 2 was due to the functions of three methyltransferase genes, *orf2*, *orfA*, and *orfB* (13, 30). In this study, we found that the serotype 13 GPL was structurally very close to those of serotypes 7 and 12, and we determined the novel structure of

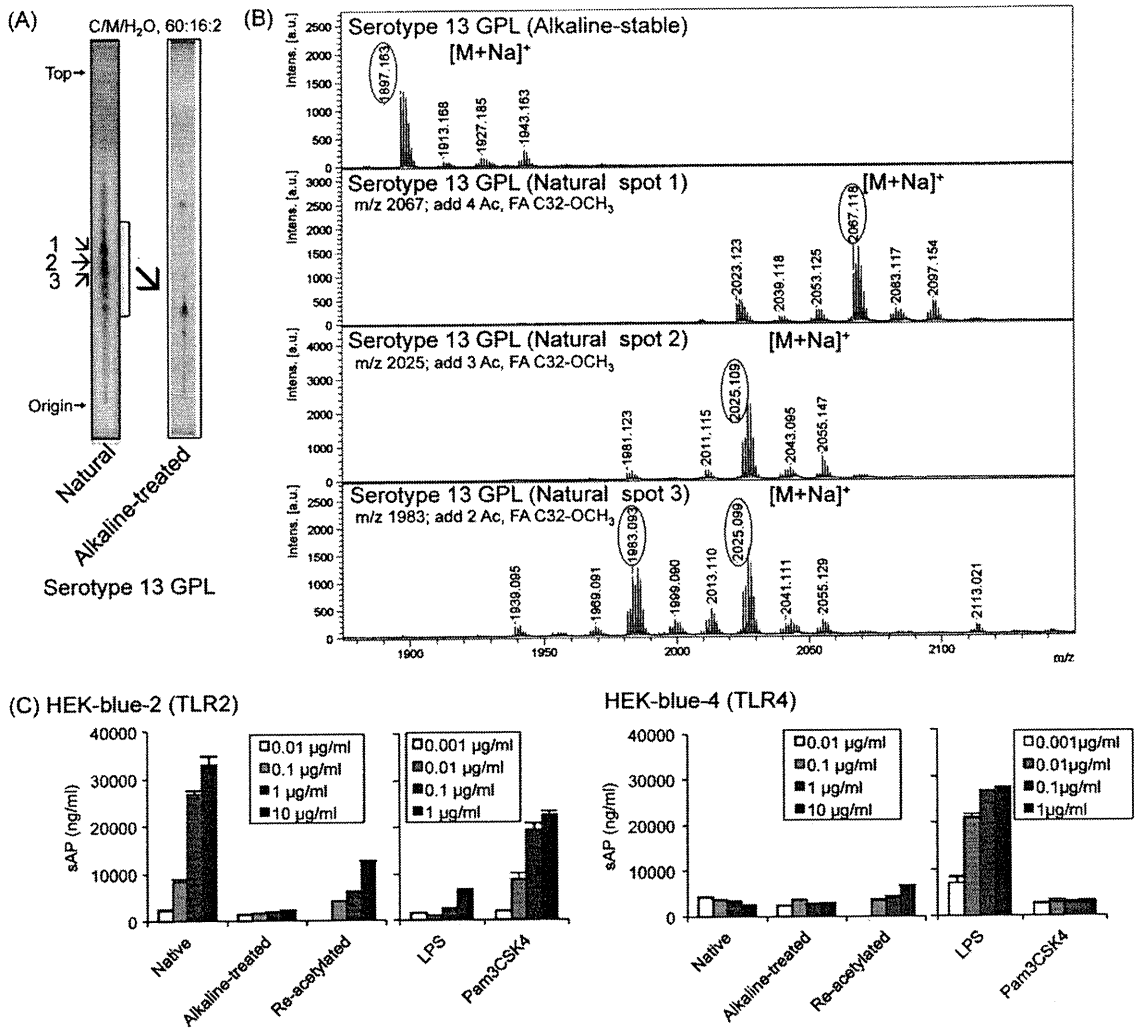

FIG. 6. TLC patterns, MALDI-TOF MS spectra, and TLR recognition of the native and alkaline-treated serotype 13 GPL. (A) The TLC plate was developed with a solvent system of chloroform-methanol-water (60:16:2 [vol/vol/vol]). Three major spots of native GPL are indicated by the numbers from top to bottom. (B) The major spots were purified and their molecular ions were measured by MALDI-TOF MS. The condition is described in the legend for Fig. 1. (C) HEK-blue-2 and -4 cells (2×10^5 cells/ml) were stimulated with native, alkaline-treated, and reacetylated serotype 13 GPLs. After 24 h of incubation, NF-κB activation was assessed by measuring the levels of secreted alkaline phosphatase (sAP) in the supernatant by using QUANTI-Blue. The data are means ± standard deviations (SD) for two experiments done in duplicate.

the serotype 13 GPL to be 4-2′-hydroxypropanoyl-amido-4,6-dideoxy-β-hexose-(1→3)-4-*O*-methyl-α-L-rhamnose-(1→3)-α-L-rhamnose-(1→3)-α-L-rhamnose-(1→2)-α-L-6-deoxy-talose. This result clarified that the serotype 13 GPL is structurally different from the serotype 7 and 12 GPLs in the *O*-methylations of the terminal *N*-acylated Hex and Rha next to the terminal Hex. Serotype 13 GPL lacked the *O*-methyl group in the terminal *N*-acylated Hex, although serotype 7 and 12 GPLs had one at the C-2 and C-3 positions, respectively. The composition and position of the *N*-acyl group at the terminal Hex were completely identical in these three GPLs. At the Rha next to the terminal Hex, serotype 12 and 13 GPLs have an *O*-methyl group at the C-4 position, and this modification is present in all group 2 GPLs except for the serotype 7 GPL, suggesting that this methyl group may play a role in MAIC physiology and virulence. These results also implied that *M. intracellulare* serotypes 7, 12, and 13 are very close phylogenetically.

We investigated the relationship between the structure and biosynthetic pathway and tried to verify the phylogenetic classification of serotypes 7, 12, and 13 by genetic analysis of GPL biosynthesis. We previously reported the nucleotide sequences of the *gtfB-drrC* region, which completely determine each serotype-specific GPL in serotypes 7 and 12 (13, 30), and found the sequence of the serotype 13 gene cluster (unpublished data). The genetic organizations of the *gtfB-drrC* regions in serotype 7, 12, and 13 gene clusters closely resemble each other. Seven common ORFs are conserved in *gtfB-drrC* clusters, suggesting that these three serotypes diverged from a common ancestor. The *orfA-orfB* region in serotypes 12 and 13 replaced *orf2* in serotype 7. Only one nucleotide substitution was found in the 1.95-kb segment in *orfA-orfB* of serotypes 12

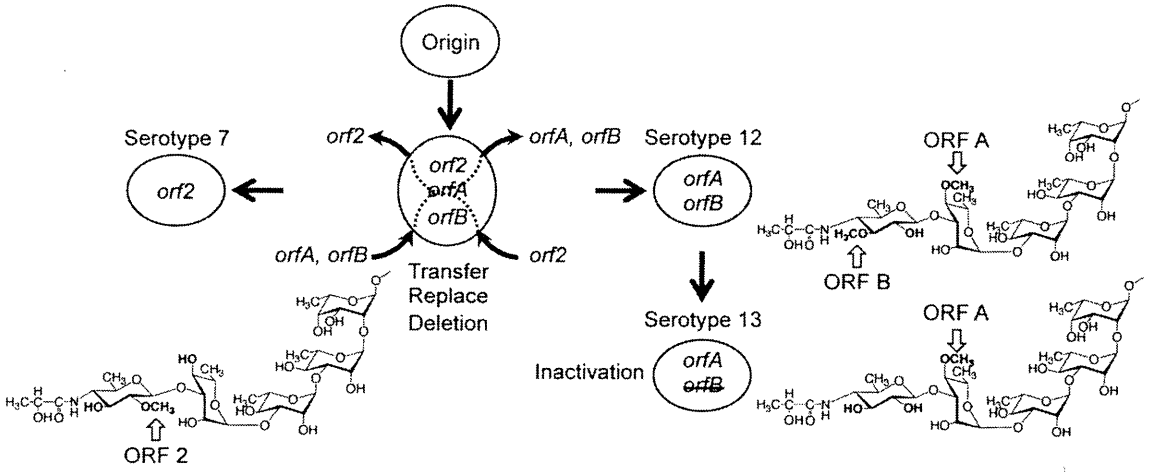

FIG. 7. Scheme of the relationship between GPL biosynthesis ORFs encoded the methyltransferases and their structures.

and 13, and *orfB* in serotype 13 was inactivated. In general, it is unusual for an ORF inactivated by a missense mutation to remain in the genome because it is a burden for the bacterium to transcribe and translate an inactivated ORF. Thus, the *M. intracellulare* serotype 13 strain must have diverged from an *M. intracellulare* serotype 12 organism recently. Serotype 13 GPL also has 4-*O*-Me-Rha. *orfA* is responsible for this methylation. In previous studies, we demonstrated that the *orfB* activity had incapacitated the *orf2* activity, which synthesizes an *O*-methyl group at the C-2 position of the terminal Hex of *M. intracellulare* serotype 7. We also showed that the *orf2* activity was independent of *orfA* activity in *M. intracellulare* serotype 12 (30). The relation of methyltransferases, *orfA*, *orfB*, and *orf2* is summarized in Fig. 7.

GPLs are correlated with colony morphology, sliding motility, biofilm formation, immune modulation, and virulence (2, 3, 16, 34). GPLs have several significant features. They are produced in MAIC species and absent from *Mycobacterium tuberculosis*, making it possible to distinguish MAIC from tuberculous mycobacteria (11, 20). An anti-GPL antibody is produced in the sera of patients and reflects the disease, which is useful in diagnosis and treatment (21, 22, 25). Moreover, it was reported that ethambutol-susceptible and -resistant MAIC strains of serotype 1 had different GPL profiles. The susceptible strain expressed only the polar serotype 1 GPL, and the resistant strain expressed several apolar GPLs. The efficacy of antibiotics may be affected by the GPL profile through differences in cell wall permeability (19). On the other hand, the importance of TLR-mediated responses has been studied in tuberculous infections. Means et al. (28) reported that *M. tuberculosis* activated both TLR2 and TLR4, whereas heat-killed *M. tuberculosis* and *M. avium* activated only TLR2. It was observed that MyD88- and TLR2-deficient mice have increased susceptibility to *M. avium* infection compared to TLR4-deficient and wild-type mice (12). These lines of evidence suggest that TLRs are related to host recognition of the MAIC components containing GPLs and affect MAIC infections. Brennan and Goren (6) first proposed that GPLs were alkaline-stable lipids and made it possible to classify serospecificity by the unique, variable deacetylated OSE sequences (9). We did not detect any biological activity of these alkaline-treated GPLs on splenocytes and bone marrow macrophages of mice in *in vitro* stimulation. Recently, Schorey and colleagues (35, 36) clarified that serotype 1 and 2 GPLs can function as TLR2 agonists and promote macrophage activation in a TLR2- and MyD88-dependent pathway. They reported that the acetylated and methylated groups of GPLs were necessary for GPL-TLR2 interaction as a molecular requirement. In this study, we purified both native and alkaline-treated serotype 13 GPLs and clarified the acetylation patterns of serotype 13 GPL. It was confirmed that the native acetylated form of serotype 13 GPL was recognized via TLR2 and that the deacetylated form by alkaline treatment was not recognized. The serotype 13 GPL has one *O*-methyl group next to the terminal *N*-acylated Hex that was stable regardless of alkaline treatment. Taken together, an acetyl rather than a methyl group was necessary for host immune response via TLR2. The completely acetylated derivative of alkaline-treated serotype 13 GPL partially recovered the HEK-blue-2 activation, compared to the native form containing 2 to 4 acetylated groups. It may be important for GPL-TLR2 interaction to balance the hydrophobicity and hydrophilicity of the molecule. Recht and Kolter (32) reported that the acetylation of GPL affects sliding motility and biofilm formation by deleting the *atf1* gene, which is responsible for acetylation on the 6-d-Tal of GPL core in *Mycobacterium smegmatis*. Rhoades et al. (33) reported that the *Mycobacterium abscessus* GPLs were related to smooth and rough colony morphology and that the GPLs in the outermost portion of the cell wall masked underlying phosphatidyl-*myo*-inositol mannosides involved in stimulating the innate immune response via TLR2. In contrast, our results suggest that the species-specific acetylated GPL is effective in host recognition as a TLR2 agonist independent of phosphatidyl-*myo*-inositol mannosides and that it plays important roles directly in host innate immune responses. Regulating the acetylation of GPL may control the MAIC pathogenicity by, for example, developing the inhibitor of ATF1.

The present study demonstrated the chemical structure and biosynthesis gene cluster of the serotype 13 GPL of *M. intracellulare* and host innate immune response via TLR2. Serotype 13 GPL should be included in group 2 GPLs, and the phylogenetic relationship of serotype 7, 12, and 13 strains was par-

tially clarified by the GPL. We propose that the lipid components in the cell envelope are important for MAIC infection and that the structure modification must be taken into account. These findings shed light on the better understanding of the structure-function relationships of GPLs and may open a new avenue for the prevention of MAIC infections.

ACKNOWLEDGMENTS

This work was supported by grants from the Ministry of Education, Culture, Sports, Science and Technology of Japan, the Japan Health Sciences Foundation, and the Ministry of Health, Labor and Welfare of Japan (Research on Emerging and Reemerging Infectious Diseases).

REFERENCES

1. **Aspinall, G. O., D. Chatterjee, and P. J. Brennan.** 1995. The variable surface glycolipids of mycobacteria: structures, synthesis of epitopes, and biological properties. Adv. Carbohydr. Chem. Biochem. **51:**169–242.
2. **Belisle, J. T., K. Klaczkiewicz, P. J. Brennan, W. R. Jacobs, Jr., and J. M. Inamine.** 1993. Rough morphological variants of *Mycobacterium avium*. Characterization of genomic deletions resulting in the loss of glycopeptidolipid expression. J. Biol. Chem. **268:**10517–10523.
3. **Bhatnagar, S., and J. S. Schorey.** 2007. Exosomes released from infected macrophages contain *Mycobacterium avium* glycopeptidolipids and are proinflammatory. J. Biol. Chem. **282:**25779–25789.
4. **Bhatt, A., et al.** 2007. Deletion of kasB in *Mycobacterium tuberculosis* causes loss of acid-fastness and subclinical latent tuberculosis in immunocompetent mice. Proc. Natl. Acad. Sci. U. S. A. **104:**5157–5162.
5. **Bozic, C. M., M. McNeil, D. Chatterjee, I. Jardine, and P. J. Brennan.** 1988. Further novel amido sugars within the glycopeptidolipid antigens of *Mycobacterium avium*. J. Biol. Chem. **263:**14984–14991.
6. **Brennan, P. J., and M. B. Goren.** 1979. Structural studies on the type-specific antigens and lipids of the *Mycobacterium avium-Mycobacterium intracellulare-Mycobacterium scrofulaceum* serocomplex. *Mycobacterium intracellulare* serotype 9. J. Biol. Chem. **254:**4205–4211.
7. **Brennan, P. J., M. Heifets, and B. P. Ullom.** 1982. Thin-layer chromatography of lipid antigens as a means of identifying nontuberculous mycobacteria. J. Clin. Microbiol. **15:**447–455.
8. **Brennan, P. J., and H. Nikaido.** 1995. The envelope of mycobacteria. Annu. Rev. Biochem. **64:**29–63.
9. **Chatterjee, D., and K. H. Khoo.** 2001. The surface glycopeptidolipids of mycobacteria: structures and biological properties. Cell. Mol. Life Sci. **58:** 2018–2042.
10. **Eckstein, T. M., J. T. Belisle, and J. M. Inamine.** 2003. Proposed pathway for the biosynthesis of serovar-specific glycopeptidolipids in *Mycobacterium avium* serovar 2. Microbiology **149:**2797–2807.
11. **Enomoto, K., et al.** 1998. Rapid serodiagnosis of *Mycobacterium avium-intracellulare* complex infection by ELISA with cord factor (trehalose 6, 6′-dimycolate), and serotyping using the glycopeptidolipid antigen. Microbiol. Immunol. **42:**689–696.
12. **Feng, C. G., et al.** 2003. Mice lacking myeloid differentiation factor 88 display profound defects in host resistance and immune responses to *Mycobacterium avium* infection not exhibited by Toll-like receptor 2 (TLR2)- and TLR4-deficient animals. J. Immunol. **171:**4758–4764.
13. **Fujiwara, N., et al.** 2007. Structural characterization of a specific glycopeptidolipid containing a novel *N*-acyl-deoxy sugar from *Mycobacterium intracellulare* serotype 7 and genetic analysis of its glycosylation pathway. J. Bacteriol. **189:**1099–1108.
14. **Fujiwara, N., et al.** 2008. Structural analysis and biosynthesis gene cluster of an antigenic glycopeptidolipid from *Mycobacterium intracellulare*. J. Bacteriol. **190:**3613–3621.
15. **Hakomori, S.** 1964. A rapid permethylation of glycolipid, and polysaccharide catalyzed by methylsulfinyl carbanion in dimethyl sulfoxide. J. Biochem. **55:**205–208.
16. **Howard, S. T., et al.** 2006. Spontaneous reversion of *Mycobacterium abscessus* from a smooth to a rough morphotype is associated with reduced expression of glycopeptidolipid and reacquisition of an invasive phenotype. Microbiology **152:**1581–1590.
17. **Kaufmann, S. H.** 2001. How can immunology contribute to the control of tuberculosis? Nat. Rev. Immunol. **1:**20–30.
18. **Khoo, K. H., et al.** 1996. Novel *O*-methylated terminal glucuronic acid characterizes the polar glycopeptidolipids of *Mycobacterium habana* strain TMC 5135. J. Biol. Chem. **271:**12333–12342.
19. **Khoo, K. H., et al.** 1999. Altered expression profile of the surface glycopeptidolipids in drug-resistant clinical isolates of *Mycobacterium avium* complex. J. Biol. Chem. **274:**9778–9785.
20. **Kitada, S., et al.** 2008. Serodiagnosis of *Mycobacterium avium*-complex pulmonary disease using an enzyme immunoassay kit. Am. J. Respir. Crit. Care Med. **177:**793–797.
21. **Kitada, S., et al.** 2010. Serodiagnosis of pulmonary disease due to *Mycobacterium avium* complex proven by bronchial wash culture. Chest **138:**236–237.
22. **Kitada, S., et al.** 2007. Serological test and chest computed tomography findings in patients with *Mycobacterium avium* complex lung disease. Eur. Respir. J. **29:**1217–1223.
23. **Krzywinska, E., J. Krzywinski, and J. S. Schorey.** 2004. Phylogeny of *Mycobacterium avium* strains inferred from glycopeptidolipid biosynthesis pathway genes. Microbiology **150:**1699–1706.
24. **Krzywinska, E., and J. S. Schorey.** 2003. Characterization of genetic differences between *Mycobacterium avium* subsp. *avium* strains of diverse virulence with a focus on the glycopeptidolipid biosynthesis cluster. Vet. Microbiol. **91:**249–264.
25. **Maekura, R., et al.** 2005. Clinical and prognostic importance of serotyping *Mycobacterium avium-Mycobacterium intracellulare* complex isolates in human immunodeficiency virus-negative patients. J. Clin. Microbiol. **43:**3150–3158.
26. **Marras, T. K., and C. L. Daley.** 2002. Epidemiology of human pulmonary infection with nontuberculous mycobacteria. Clin. Chest Med. **23:**553–567.
27. **Matsunaga, I., T. Komori, A. Ochi, N. Mori, and M. Sugita.** 2008. Identification of antibody responses to the serotype-nonspecific molecular species of glycopeptidolipids in *Mycobacterium avium* infection. Biochem. Biophys. Res. Commun. **377:**165–169.
28. **Means, T. K., et al.** 1999. Human Toll-like receptors mediate cellular activation by *Mycobacterium tuberculosis*. J. Immunol. **163:**3920–3927.
29. **Miyamoto, Y., et al.** 2010. Novel rhamnosyltransferase involved in biosynthesis of serovar 4-specific glycopeptidolipid from *Mycobacterium avium* complex. J. Bacteriol. **192:**5700–5708.
30. **Nakata, N., et al.** 2008. Identification and characterization of two novel methyltransferase genes that determine the serotype 12-specific structure of glycopeptidolipids of *Mycobacterium intracellulare*. J. Bacteriol. **190:**1064–1071.
31. **Primm, T. P., C. A. Lucero, and J. O. Falkinham III.** 2004. Health impacts of environmental mycobacteria. Clin. Microbiol. Rev. **17:**98–106.
32. **Recht, J., and R. Kolter.** 2001. Glycopeptidolipid acetylation affects sliding motility and biofilm formation in *Mycobacterium smegmatis*. J. Bacteriol. **183:**5718–5724.
33. **Rhoades, E. R., et al.** 2009. *Mycobacterium abscessus* glycopeptidolipids mask underlying cell wall phosphatidyl-myo-inositol mannosides blocking induction of human macrophage TNF-alpha by preventing interaction with TLR2. J. Immunol. **183:**1997–2007.
34. **Schorey, J. S., and L. Sweet.** 2008. The mycobacterial glycopeptidolipids: structure, function, and their role in pathogenesis. Glycobiology **18:**832–841.
35. **Sweet, L., and J. S. Schorey.** 2006. Glycopeptidolipids from *Mycobacterium avium* promote macrophage activation in a TLR2- and MyD88-dependent manner. J. Leukoc. Biol. **80:**415–423.
36. **Sweet, L., et al.** 2008. *Mycobacterium avium* glycopeptidolipids require specific acetylation and methylation patterns for signaling through Toll-like receptor 2. J. Biol. Chem. **283:**33221–33231.
37. **Tsang, A. Y., J. C. Denner, P. J. Brennan, and J. K. McClatchy.** 1992. Clinical and epidemiological importance of typing of *Mycobacterium avium* complex isolates. J. Clin. Microbiol. **30:**479–484.
38. **Tsang, A. Y., I. Drupa, M. Goldberg, J. K. McClatchy, and P. J. Brennan.** 1983. Use of serology and thin-layer chromatography for the assembly of an authenticated collection of serovars within the *Mycobacterium avium-Mycobacterium intracellulare-Mycobacterium scrofulaceum* complex. Int. J. Syst. Bacteriol. **33:**285–292.
39. **Wagner, D., and L. S. Young.** 2004. Nontuberculous mycobacterial infections: a clinical review. Infection **32:**257–270.

ANTIMICROBIAL AGENTS AND CHEMOTHERAPY, Sept. 2011, p. 4000–4005 Vol. 55, No. 9
0066-4804/11/$12.00 doi:10.1128/AAC.00434-11

Apoptosis-Inducing Activity of Clofazimine in Macrophages[▽]

Yasuo Fukutomi,* Yumi Maeda, and Masahiko Makino

Leprosy Research Center, National Institute of Infectious Diseases, 4-2-1, Aoba-cho, Higashimurayama-shi, Tokyo 189-0002, Japan

Received 1 April 2011/Returned for modification 19 May 2011/Accepted 9 June 2011

Clofazimine is a riminophenazine compound which has been used for the treatment of leprosy since the 1960s. Although the drug is effective in the management of leprosy reactions because of its anti-inflammatory activity, the mechanism leading to the cessation of inflammation is not well understood. In the present study, it was shown that clofazimine exhibits apoptosis-inducing activity in macrophages. When human monocyte-derived macrophages were cultured *in vitro* in the presence of clofazimine, the cells exhibited a marked decrease in metabolic activity and showed shrinkage in cell size, indicating cell death. Nuclear condensation and fragmentation were also observed by Giemsa and Hoechst 33248 stains. The endonuclease inhibitor $ZnCl_2$ inhibited the clofazimine-induced cell death. Significant enhancement of caspase-3 activity was observed in clofazimine-treated macrophages and THP-1 cells. Collectively, these results suggest the apoptosis-inducing activity of clofazimine in macrophages, which may also be responsible for the antibacterial properties of clofazimine.

Clofazimine (B663) is a phenazine iminoquinone derivative, specifically, a riminophenazine dye with the empirical formula $C_{27}H_{22}C_{12}$. In the 1950s, Barry et al. synthesized a large number of compounds by progressive chemical alteration of the anilinoaposafranine molecule, several of which showed antituberculous activity both *in vitro* and in experimental animals (1). Of these compounds, clofazimine (or Lamprene or B663) was found to be highly active against mycobacteria with the least toxicity. Chang (4) observed the antibacterial activity of clofazimine against *Mycobacterium lepraemurium* at about the same time as its anti-*M. leprae* activity was reported by Browne (2) and Browne and Hogenzeil (3). Later, after the introduction of the mouse footpad method of Shepard and Chang (22), its antibacterial activity against *M. leprae* was demonstrated (18).

Clofazimine has bifunctional activity: antibacterial and anti-inflammatory. It was used in the treatment of leprosy for its antibacterial action against *M. leprae*. Later, it was also found to possess an anti-inflammatory action which makes it a very useful drug in the treatment of acute reactions, including erythema nodosum leprosum (ENL), neuritis, iritis, etc., although its mechanism of action is unknown (2). *In vitro* studies on the effect of clofazimine on immune cells have been conducted. Clofazimine increases superoxide anion production and degranulation by stimulated neutrophils. and tumor necrosis factor alpha (TNF-α) potentiates this enhancement (15). The mechanism underlying this pro-oxidative effect seems to involve stimulation of phospholipase A2 (PLA2) activity with subsequent accumulation of arachidonic acid and lysophospholipids, which act as second messengers to activate oxidase (10). In addition, a number of reports have demonstrated the effects of clofazimine that might predict increased immune activity. Lysosomal enzyme activity of cultured macrophages was upregulated by clofazimine (21). Peripheral blood monocytes from healthy volunteers have been demonstrated to exhibit increased major histocompatibility complex class II expression following incubation with clofazimine (25). Increased oxygen uptake during phagocytosis was observed in neutrophils derived from patients with pyoderma gangrenosum during clofazimine therapy (5). Suppressor T-cell activity was decreased in mycobacteria-infected mice during clofazimine treatment (26). However, the mechanisms underlying the anti-inflammatory action of clofazimine are still unclear.

In the present study, we examined the effect of clofazimine on macrophages and found that the drug possessed apoptosis-inducing activity.

MATERIALS AND METHODS

Drug and chemicals. Clofazimine (Sigma-Aldrich Co., St. Louis, MO), rifampin (catalog no. R3501; Sigma-Aldrich Co.), and dapsone (DDS; Biomol Research Inc., Butler Pike Plymouth Meeting, PA) were dissolved in dimethyl sulfoxide (DMSO) and stored at −30°C until use. Ampicillin was obtained from Sigma-Aldrich Co.

Culture of human macrophages and isolation of bacilli. Human peripheral blood was obtained under informed consent from healthy individuals. Peripheral blood mononuclear cells (PBMCs) were isolated using Ficoll-Paque Plus (GE Healthcare Life Sciences, Buckinghamshire, United Kingdom) gradient centrifugation (12). The cells were suspended in AIM-V medium (Gibco BRL, Invitrogen Corp., Carlsbad, CA), and 1×10^6 PBMCs were cultured in a well of a 24-well tissue culture plate (Falcon; Becton Dickinson Labware, Becton Dickinson and Company, Franklin Lakes, NJ) containing 13-mm round coverslips (Nunc Thermanox coverslips; Nalge Nunc, Thermo Scientific, Rochester, NY) at 37°C in a 5% CO_2 incubator for adherence of monocytes. After 1 h incubation, the coverslips were washed with Hanks' balanced salt solution (HBSS; Sigma-Aldrich Co.) to remove nonadherent cells. The monocytes on the coverslips were cultured in a new 24-well plate containing RPMI 1640 medium (Sigma-Aldrich Co.) supplemented with 25 mM HEPES, 10% fetal bovine serum (FBS; Bio Whittaker Co., Walkersville, MD), 2 mM L-glutamine, and 100 μg/ml ampicillin (RPMI-10F) in the presence of 40 ng/ml of granulocyte-macrophage colony-stimulating factor (R&D Systems, Minneapolis, MN). After 10 days, the cells were differentiated into macrophages and used for experiments. In some experiments, PBMCs were cultured in 35-mm cell culture dishes (Corning Inc., Corning, NY) for adherence, and adherent monocytes were cultured for 10 days. Human monocytic leukemia cell line THP-1 was maintained in RPMI 1640 medium containing 15% fetal bovine serum.

* Corresponding author. Mailing address: Leprosy Research Center, National Institute of Infectious Diseases, 4-2-1, Aoba-cho, Higashimurayama-shi, Tokyo 189-0002, Japan. Phone: 81-42-391-8211. Fax: 81-42-394-9092. E-mail: fukutomi@nih.go.jp.

▽ Published ahead of print on 20 June 2011.

M. leprae (Thai-53 strain) was isolated from the footpads of BALB/c *nu/nu* mice that had been inoculated with *M. leprae* 8 months prior to isolation, and the bacillary number was enumerated according to the method of Shepard and Chang (22).

Light and phase-contrast microscopy. Macrophages on the coverslip were fixed with absolute methanol, followed by performing Giemsa stain (Wako Co., Japan). After they were mounted on a glass slide, the cells were observed under a light microscope (Optiphot-2; Nikon Co., Tokyo, Japan). Photographs were taken with a digital camera (Nikon F70s). Macrophages in 35-mm dishes were incubated in the presence of clofazimine and observed under a phase-contrast microscope (Olympus CKX41 with ×10- and ×20-objective lenses). Photographs were taken with an Olympus DP50 system. Image acquisition and data processing were done using the DP controller software.

Fluorescence microscopy. Fluorescence staining for DNA was employed. Macrophages were cultured in an 8-well chamber slide (Lab-Tek II chamber slide system; Nalge Nunc). The cells were incubated in the presence of clofazimine and subsequently fixed with 2.5% glutaraldehyde in phosphate-buffered saline (PBS). Hoechst 33342 dye (Sigma-Aldrich Co.) in PBS was added to the wells at a final concentration of 10 μM, and the slide was incubated for 1 h at 37°C. The cells on the slide were observed under a fluorescence microscope (Olympus BX60 with a ×40-objective lens) equipped with an Olympus DP50 system. The digital images were processed with DP controller software.

Determination of cell death. Cell viability was determined using the colorimetric method (Cell Titer 96 aqueous nonradioactive cell proliferation assay; Promega Corp., Madison, WI). Briefly, cells in a 24-well plate were incubated in the presence of clofazimine in phenol red-free RPMI 1640 medium containing 10% FBS, followed by addition of 3-(4,5-dimethylthiazol-2-yl)-5-(3-carboxymethoxyphenyl)-2-(4-sulfophenyl)-2*H*-tetrazolium, inner salt/phenazine methosulfate solution (formazan reagent). After 1 h incubation at 37°C, an aliquot of medium was transferred into a well of a 96-well plate, and the developed color was measured by a microplate reader at 490 nm. In addition, the activity of lactate dehydrogenase (LDH), released from dead cells into culture supernatants, was measured by a colorimetric assay (Cytotox 96 nonradioactive cytotoxicity assay; Promega Corp.). The color that developed in a sample incubated with LDH substrate was measured by a microplate reader at 490 nm (Vmax; Molecular Devices Corp., Sunnyvale, CA).

DNA electrophoresis. THP-1 cells or macrophages were harvested from the culture, and DNA was purified by a spin column method (E.Z.N.A. tissue DNA kits; Omega Bio-Tek, Norcross, GA). Briefly, 5×10^6 cells incubated in the presence of clofazimine were harvested, centrifuged at 2,000 rpm for 5 min, washed once with PBS, and resuspended in PBS. Protease was added, the mixture was heated at 65°C for 5 min, and buffer BL was added. After the mixture was heated at 70°C for 10 min, ethanol was further added. The mixture was applied to a HiBind spin column and centrifuged. DNA bound to the column was finally eluted, and the DNA preparation was subjected to electrophoresis in a 1% agarose gel, followed by ethidium bromide staining, and DNA was visualized by UV transillumination.

Western blotting. THP-1 cells or macrophages incubated with clofazimine were washed once with PBS(−) and lysed in lysis buffer (CelLytic-M; Sigma-Aldrich Co.) containing 2 protease inhibitor cocktails (phosphatase inhibitor cocktail 1 and phosphatase inhibitor cocktail 2; Sigma-Aldrich Co.). In the case of clofazimine-treated adherent macrophages, the cells were scraped off the dishes with a rubber policeman. The lysates were incubated for 10 min on ice and centrifuged at 13,000 rpm for 5 min. The protein concentration was determined. Ten micrograms of total protein was loaded onto an SDS-PAGE gel. After running the electrophoresis, the proteins in the gel were transferred onto an Immobilon PSQ membrane (Millipore Corporation, Billerica, MA). After washing with Tris-buffered saline (2.42 g Tris base and 8 g NaCl per 1 liter, pH 7.6) containing 0.05% Tween 20 (TBS-T), the membrane was blocked with 5% skim milk (Amersham ECL Plus Western blotting reagent pack; GE Healthcare Life Sciences, Amersham Place, Buckinghamshire, United Kingdom) for 1 h at room temperature. The membrane was washed 3 times with TBS-T and incubated overnight with 1:3,000-diluted primary anticleaved caspase-3 antibody (cleaved caspase antibody sampler kit; Cell Signaling Technology Inc., Danvers, MA). The membrane was then incubated with 1:10,000-diluted horseradish peroxidase (HRP)-conjugated secondary antibody for 1 h at room temperature. Finally, proteins were detected by incubating the membrane with HRP substrate (Immobilon Western chemiluminescent HRP substrate; Millipore Corporation), and the membrane was exposed to X-ray film (Amersham Hyperfilm ECL; GE Healthcare). For reprobing of the membrane, the membrane was washed with TBS-T and incubated with stripping buffer (Restore Plus Western blot stripping buffer; Pierce, IL). After the membrane was blocked, it was used again for probing different antibodies, such as cleaved caspase-9 and poly(ADP-ribose) polymerase (PARP) antibodies (cleaved caspase antibody sampler kit; Cell Signaling Technology Inc.) and beta-actin antibody (Cell Signaling Technology Inc.).

Colorimetric caspase assay. Colorimetric substrates for caspases were used to determine caspase-3 activity (colorimetric caspase assay kits; Biovision Research Products, CA) in lysates of cells incubated in the presence of clofazimine. Briefly, 5×10^6 cells were pelleted and lysed with chilled lysis buffer. After centrifugation, the supernatant was transferred to a new tube, and reaction buffer and a substrate for caspase-3, Asp-Glu-Val-Asp–*p*-nitroanilide, were added to the tube. After incubation for 2 h at 37°C, the samples were transferred into a well of a 384-well plate and read by a plate reader at 405 nm (Infinite F200; Tecan Systems Inc., San Jose, CA). The background reading was obtained by subtracting the reading for the reaction buffer from the reading for the lysate samples.

PGE_2 assay. The amount of prostaglandin E_2 (PGE_2) in the culture supernatants was measured by enzyme-linked immunosorbent assay (catalog no. 514010; Cayman Chemical Co., MI).

RESULTS

Morphological changes observed after treatment with clofazimine. Macrophages differentiated from human monocytes were incubated in the presence of 10 μg/ml of clofazimine for 20 h. The change in cell morphology was observed under a phase-contrast microscope. As shown in Fig. 1B, in the presence of clofazimine, the cells exhibited shrinkage in cell size and membrane blebbing. The death of more than 80% of cells was observed (Fig. 1B). As a control, Fig. 1A shows the normal morphology of macrophages. By Giemsa stain, too, these clofazimine-treated cells exhibited shrinkage in cell size, accompanied by the appearance of fragmented smaller nuclei (arrow in Fig. 1D), suggesting the apoptotic nature of the cells. Nontreated macrophages showed intact nuclei (arrow in Fig. 1C). Again, the change of nuclear structure was confirmed by Hoechst dye staining. Under a fluorescence microscope, nuclear condensation and membrane blebbing were observed in the clofazimine-treated cells (Fig. 1F and G), in contrast to normal cells, which showed intact nuclei (Fig. 1E). Similar fragmentation or condensation of chromatin was observed in THP-1 cells (data not shown). Such morphological changes were not observed in THP-1 cells treated with rifampin or dapsone at a concentration up to 50 μg/ml. Also, DMSO, which was used as a solvent for clofazimine at a concentration of 0.2%, had no effect on cell morphology or cell functions (negative control).

Cell death-inducing activity of clofazimine determined by colorimetric assay. Cell death was determined by a biochemical analysis using a colorimetric method. The conversion of the tetrazolium compound into soluble formazan is accomplished by metabolically active cells. When higher concentrations up to 10 μg/ml of clofazimine were employed in macrophage cultures, decreased color intensity of soluble formazan was observed, indicating cell death (Fig. 2A). Cell death was also observed in THP-1 cells (Fig. 2B). Hansen's disease is caused by infection of macrophages with *M. leprae*; therefore, we are curious to know whether *M. leprae* infection affects the cell death-inducing activity of clofazimine. When we infected macrophages with *M. leprae* at a multiplicity of infection (MOI) of 10 or 30, we found no significant difference in the induction of cell death in the presence of 10 μg/ml clofazimine, indicating that the bacilli did not inhibit or enhance clofazimine-induced cell death (Fig. 2C). Another method of determining cell death is by measurement of LDH release from

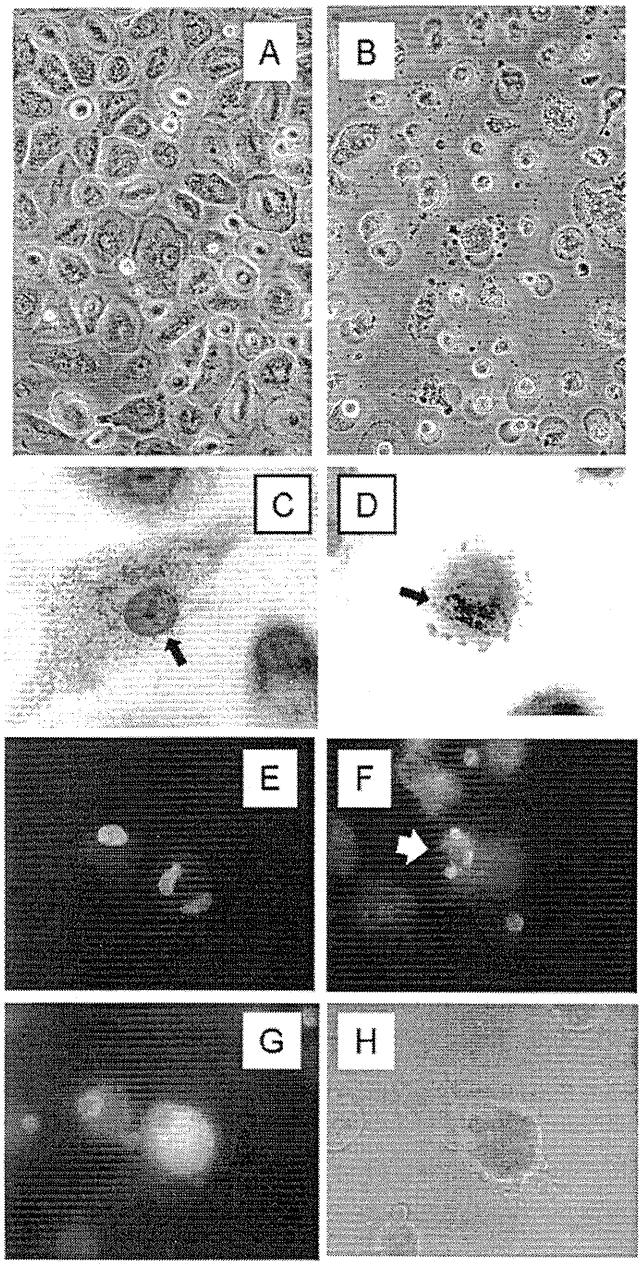

FIG. 1. Cell death induced in macrophages by clofazimine. Photographs were taken under a phase-contrast microscope (A and B) with a ×20-objective lens. (B) Human monocyte-derived macrophages were incubated in the presence of 10 μg/ml of clofazimine for 20 h. (A) Cells cultured in the absence of clofazimine showed normal morphology. Giemsa stain of clofazimine-treated macrophages was also performed (C and D). Human monocyte-derived macrophages were incubated in the presence of 10 μg/ml of clofazimine (D) or in the absence of clofazimine (C) for 24 h. Photographs were taken under a light microscope with a ×100-objective lens. Fragmentation of the nucleus was significant in the clofazimine-treated cells (arrow in panel D), in contrast to the intact morphology of the nucleus in normal cells (arrow in panel C). Nuclear condensation and fragmentation of clofazimine-treated macrophages were also confirmed under a fluorescence microscope (E to G). Macrophages were incubated in the presence of 10 μg/ml of clofazimine, followed by fixation and stained with a nucleus-staining dye, Hoechst 33342. The cells were observed under a fluorescence microscope (×40-objective lens). Cells cultured without clofazimine (E), clofazimine-treated cells (F and G), and a phase-contrast image of panel G (H) are shown.

dead cells. As shown in Fig. 3, more LDH release was observed in the manner dependent on the concentration of clofazimine.

Clofazimine treatment induces DNA ladder formation in macrophages. We examined the condition of DNA in clofazimine-treated THP-1 cells. Agarose gel electrophoresis showed fragmentation of DNA into integer multiples of 180 bp, a so-called DNA ladder (Fig. 4A), suggesting that DNA endonuclease was activated by clofazimine treatment. Therefore, we examined the effect of one of the apoptosis inhibitors, $ZnCl_2$, which is known to possess suppressing activity for endonuclease, and found that clofazimine-induced DNA fragmentation in THP-1 cells was completely blocked by $ZnCl_2$ treatment even at a low concentration of 0.25 mM $ZnCl_2$ (Fig. 4B), although it is still not clear whether $ZnCl_2$ can directly block the activity of clofazimine. Moreover, it was evident that neither cell death nor DNA fragmentation was induced by other antileprosy drugs, such as DDS or rifampin (Fig. 4C).

Clofazimine-induced cell death is mediated by activation of caspase-3. Caspases are known to be central regulators of apoptotic cell death, and caspase-3, which locates downstream of the caspase pathway, is one of the key executioners of apoptosis. Upon apoptotic stimulation, caspases are cleaved into active fragments. Figure 5 shows a Western blot analysis of extracts from THP-1 cells and macrophages cultured in the presence of clofazimine. Enhanced expression of cleaved caspase-3 was detected in cells (Fig. 5A and B). In addition, caspase-9 was also cleaved. A DNA-repairing enzyme, PARP, which is cleaved by caspase-3, was significantly activated in clofazimine-treated THP-1 cells (Fig. 5A). We next measured the caspase activity by colorimetric assay (Fig. 5C). The induction of caspase-3 by clofazimine was significantly high in macrophages as well as THP-1 cells.

Clofazimine enhanced PGE_2 production in *M. leprae*-infected macrophages. Monocyte-derived macrophages were preincubated in the presence of clofazimine for 4 h, followed by replenishment with *M. leprae*-containing medium for 20 h. The culture supernatants were collected, and the PGE_2 concentration was measured. As shown in Fig. 6, clofazimine clearly enhanced PGE_2 production in macrophages.

DISCUSSION

Riminophenazines are structurally phenazine compounds which were derived from lichens historically and were targeted for treatment of tuberculosis. The first clinically developed phenazine compound was clofazimine, whose activity has been extended to other mycobacterial diseases (1, 17). In test animals, the drug was found to inhibit the growth of mycobacteria *in vivo*, as well as *in vitro* (22), but the molecular mechanism of clofazimine in inducing anti-*M. leprae* activity is still not yet clear.

In the present study, it was found that both human monocyte-derived macrophages and THP-1 cells exhibited marked decreases in their metabolic activity in the presence of 10 μg/ml clofazimine. Under a phase-contrast microscope, 80% of the cells showed irregular morphology with shrinkage in cell size, and by a precise time course study, it was revealed that the morphological changes were evident from 6 h incubation with clofazimine. From this early time point, the cell body began to shrink, accompanied by membrane blebbing, which was also

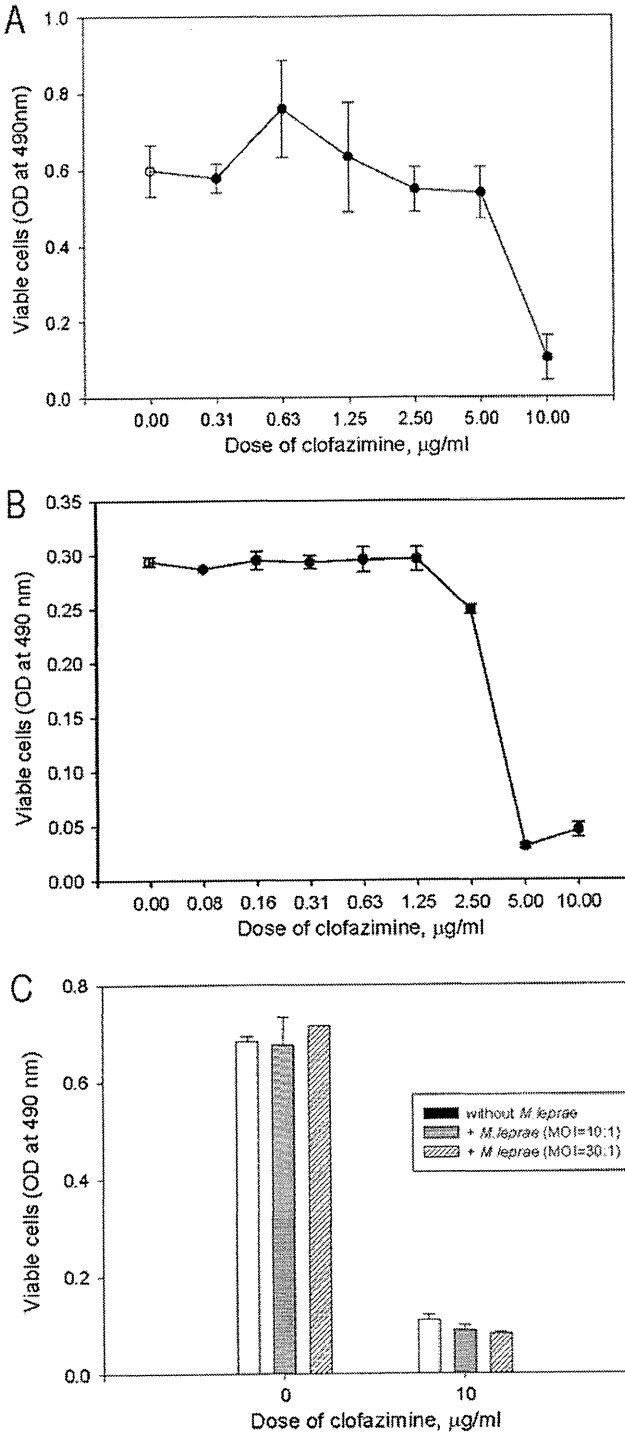

FIG. 2. Clofazimine-induced cell death in macrophages and THP-1 cells. Human monocyte-derived macrophages (A) and THP-1 cells (B) were incubated with various concentrations of clofazimine for 24 h, followed by determination of viable cells by the Cell Titer 96 cell proliferation assay. The results are representative of three independent cell culture tests. The cell death-inducing effect of clofazimine in the presence of *M. leprae* was also examined. Monocyte-derived macrophages were infected with *M. leprae* at an MOI of 10 or 30 per cell for 24 h. The infected cells were further incubated with 10 μg/ml clofazimine for another 24 h, followed by determination of viable cells by Cell Titer 96 cell proliferation assay (C). The results are representative of three independent cell culture tests. OD, optical density.

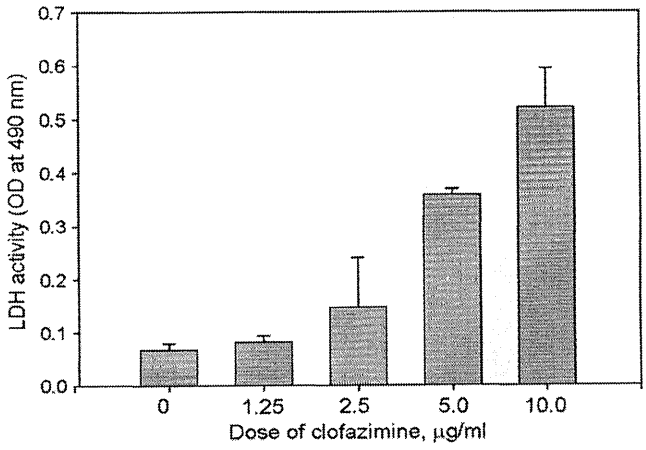

FIG. 3. LDH release from clofazimine-treated macrophages. Human monocyte-derived macrophages were incubated in the presence of the indicated concentrations of clofazimine for 24 h, and the LDH activity was measured. The results were obtained from triplicate cultures and are representative of three independent cell culture tests. OD, optical density.

evident from Giemsa stain and Hoechst staining of the nuclei (Fig. 1). Interestingly, the dose of clofazimine (10 μg/ml) required to cause cell death was equivalent to the dose required to exhibit anti-*M. leprae* activity *in vitro* by radiorespirometry (data not shown), the dose of which is in concordance with the dose required to kill *M. leprae* reported by Franzblau and O'Sullivan (7). Moreover, in our study, at 5-μg/ml concentrations of clofazimine, *M. leprae* viability was lowered in *in vitro* experiments with *M. leprae*-infected macrophages, and with this dose, *M. leprae* was found not to inhibit clofazimine-induced cell death. Therefore, clofazimine might inhibit mycobacterial growth through an alternative way by inducing apoptosis of host cells. Although the concentration of clofazimine in sera of patients taking regular doses of the drug is as low as 1 to 2 μg/ml, fat-soluble clofazimine readily accumulates in cells. In one patient, 7 months treatment with clofazimine (200 mg/day) resulted in accumulation of needle-shaped crystal inclusions in his alveolar macrophages (20). In another report, clofazimine-induced crystal-storing histiocytosis was observed in a leprosy patient (23). So, we are of the opinion that in some cells, the concentration of clofazimine is higher (10 to 20 μg/ml) than in others, so we have used a concentration of 10 μg/ml for our experiments.

Normally, cells undergo distinct morphological changes when they progress through either necrosis or apoptosis. Necrosis occurs when cells are exposed to an extreme variance from physiological conditions, resulting in damage to the plasma membrane. As such, necrosis is characterized by cell swelling and disruption of cellular organelles, with little change in the chromatin initially. In contrast, apoptotic cells shrink in size, undergo membrane blebbing, and exhibit marked alterations in their chromatin structure at an early stage under normal physiological conditions. As mentioned earlier, treatment with clofazimine resulted in highly condensed chromatin within the nucleus and membrane blebbing, indicating macrophages undergoing apoptosis. To confirm this, DNA from clofazimine-treated THP-1 cells was examined. Fragmented DNA was

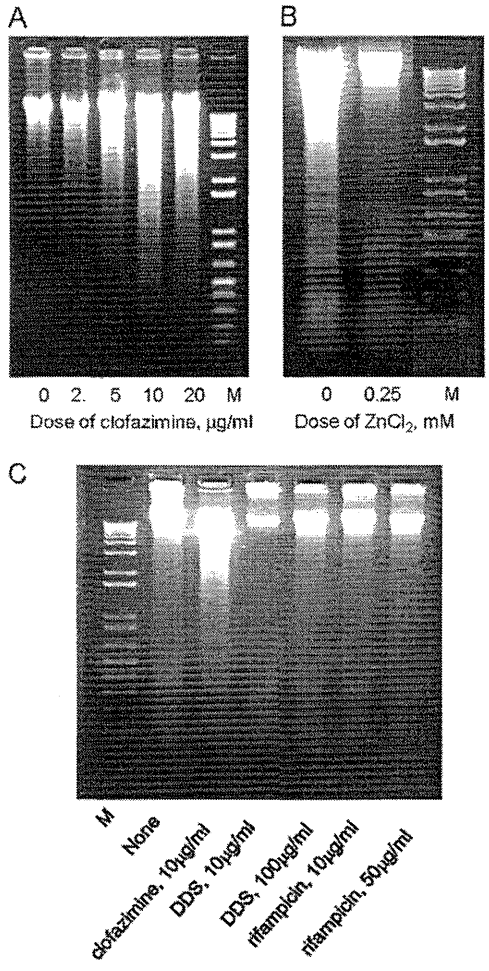

FIG. 4. DNA ladder formation in clofazimine-treated THP-1 cells and effects of other antileprosy drugs on DNA ladder formation. (A) THP-1 cells were incubated in the presence of the indicated concentrations of clofazimine for 4 h, followed by purification of DNA for agarose gel electrophoresis. An ethidium bromide-stained agarose gel is shown. (B) An endonuclease inhibitor, $ZnCl_2$, was examined for its effect on clofazimine-induced ladder formation. THP-1 cells were incubated in the presence of 10 μg/ml clofazimine and $ZnCl_2$ for 4 h. DNA was purified for electrophoresis. (C) THP-1 cells were incubated in the presence of clofazimine, DDS, and rifampin for 4 h, followed by purification of DNA. An ethidium bromide-stained agarose gel is shown. Lanes M, molecular weight marker.

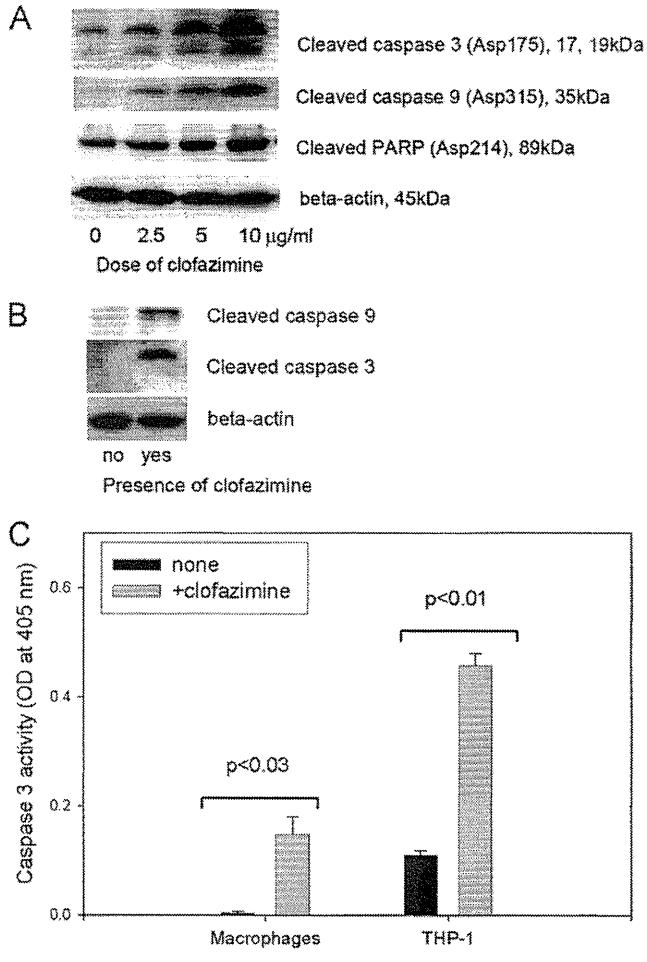

FIG. 5. Expression of caspase in clofazimine-treated THP-1 cells and macrophages. THP-1 cells were incubated in the presence of the indicated concentrations of clofazimine for 6 h, and cell lysates were processed for detection of cleaved caspase-3, caspase-9, and PARP by Western blotting (A). Similarly, monocyte-derived macrophages were incubated in the presence of 10 μg/ml of clofazimine, and the cell lysates were examined for cleaved caspase-3 and caspase-9 expression (B). The caspase activity in clofazimine-treated macrophages and THP-1 cells was analyzed. Macrophages were incubated in the presence of 10 μg/ml of clofazimine for 6 h, and the caspase-3 activity in the cell lysates was determined by colorimetric assay (C). The results are representative of three independent cell culture tests.

demonstrated, suggesting that DNA endonuclease was activated causing apoptosis.

We observed that *M. leprae* by itself does not induce apoptosis of human cells. Similarly, infection of mouse macrophages with viable *M. leprae* was shown not to induce apoptosis (11). Although apoptosis is induced when macrophages infected with *M. leprae* are treated with clofazimine, the host cell viability does not change significantly in the presence of *M. leprae*. Nevertheless, the viability of *M. leprae* in macrophages was significantly lower in clofazimine-treated cells than infected cells not treated with clofazimine (data not shown). Therefore, we can speculate that clofazimine induces apoptosis of *M. leprae*-infected macrophages, which in turn inhibits *M. leprae* growth.

Consequently, we investigated the pathways involved in the execution of macrophage apoptosis (6, 14). We observed enhanced expression of cleaved caspase-3, caspase-9, and PARP following clofazimine treatment in THP-1 cells (Fig. 5A). Colorimetric assay also indicated enhanced caspase-3 activity in both macrophages and THP-1 cells treated with clofazimine (Fig. 5C), suggesting the involvement of caspases in clofazimine-induced apoptosis.

Apoptosis has been shown to be effective in therapy of chronic inflammatory diseases (16). An immunomodulatory drug, thalidomide, is used for treatment of ENL in leprosy patients, and its anti-inflammatory activity is believed to be through the downregulation of production of the proinflammatory cytokine TNF-α (19). Gockel et al. showed that thalidomide induces apoptosis in human monocytes (8). Clofazimine